Electronic Supplementary Material (ESI) for Inorganic Chemistry Frontiers.

Supplementary Information For:

Electrophilicity Modulated Targeted Luminescence of MOF Coated Cotton Composite for Dual Analyte Detection in Aqueous Medium

*Abhijeet Rana and Shyam Biswas**

Department of Chemistry, Indian Institute of Technology Guwahati, Guwahati, 781039 Assam, India.

*To whom correspondence should be addressed. E-mail: sbiswas@iitg.ac.in; Tel: 91-3612583309.

Materials and Characterization Methods:

All the chemicals were purchased from commercial sources and used without further purification. A Bruker Avance III 600 NMR spectrometer was utilized for recording ^{1}H NMR and ^{13}C NMR spectra at 500 MHz. The mass spectrum (in -ve ESI mode) was measured with a BRUKER AUTOFLEX SPEED high-resolution mass spectrometer. Fourier transform infrared (FT-IR) spectroscopy data were recorded in the region 400-4000 cm^{-1} at room temperature with the Perkin Elmer Spectrum Two FT-IR spectrometer. The following indications were used to indicate the corresponding absorption bands: very strong (vs), strong (s), medium (m), weak (w), shoulder (sh) and broad (br). Thermogravimetric analysis (TGA) was carried out with a Perkin Elmer TGA 4000 thermal analyzer in the temperature range of 30-700 °C under N_2 atmosphere at the rate of 4 °C min^{-1}. Powder X-ray diffraction (PXRD) data were collected in transmission mode using a Bruker D2 Phaser X-ray diffractometer (30 kV, 10 mA) using Cu-*K*α (λ = 1.5406 Å) radiation. The specific surface area for N_2 sorption was calculated on a Quantachrome Autosorb iQMP gas sorption analyzer at -196 °C. FE-SEM images were collected with a Zeiss (Sigma 300) scanning electron microscope. The compound was activated at 100 °C for 24 h under a dynamic vacuum. The solid-state UV-Vis spectra were measured using UV-2600 spectrophotometer. Fluorescence emission studies were performed at room temperature using a HORIBA JOBIN YVON Fluoromax-4 spectrofluorometer.

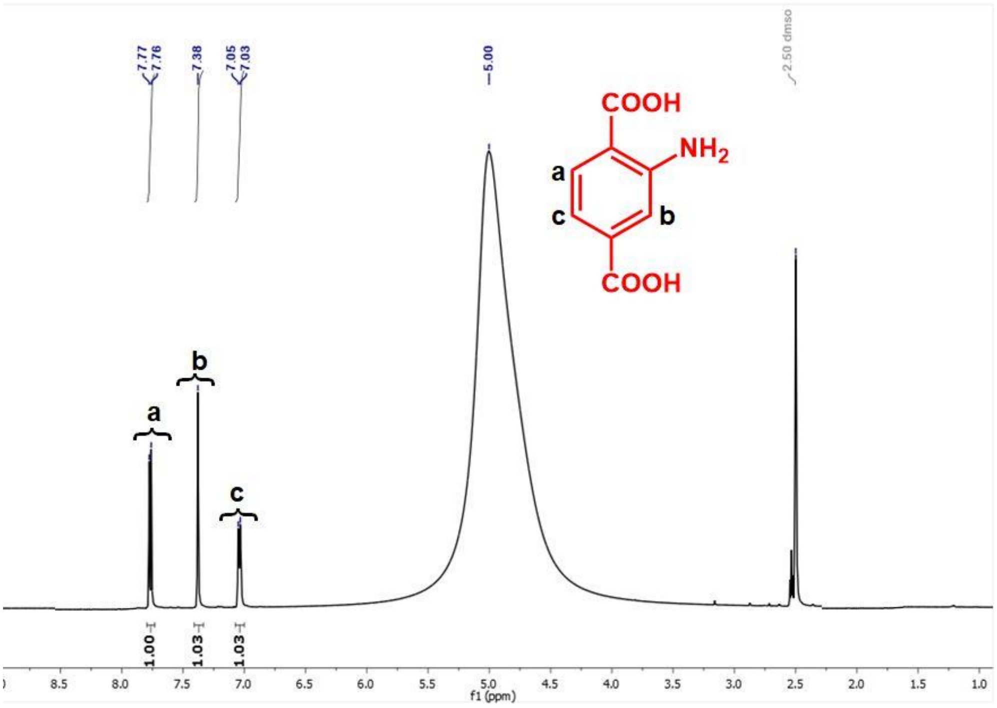

Figure S1. Digested ^{1}H NMR spectrum of **Hf-UiO-66-NH$_2$** (digested using 10 µL of 40% HF in 500 µL of DMSO-D_6 and 20 mg of MOF).

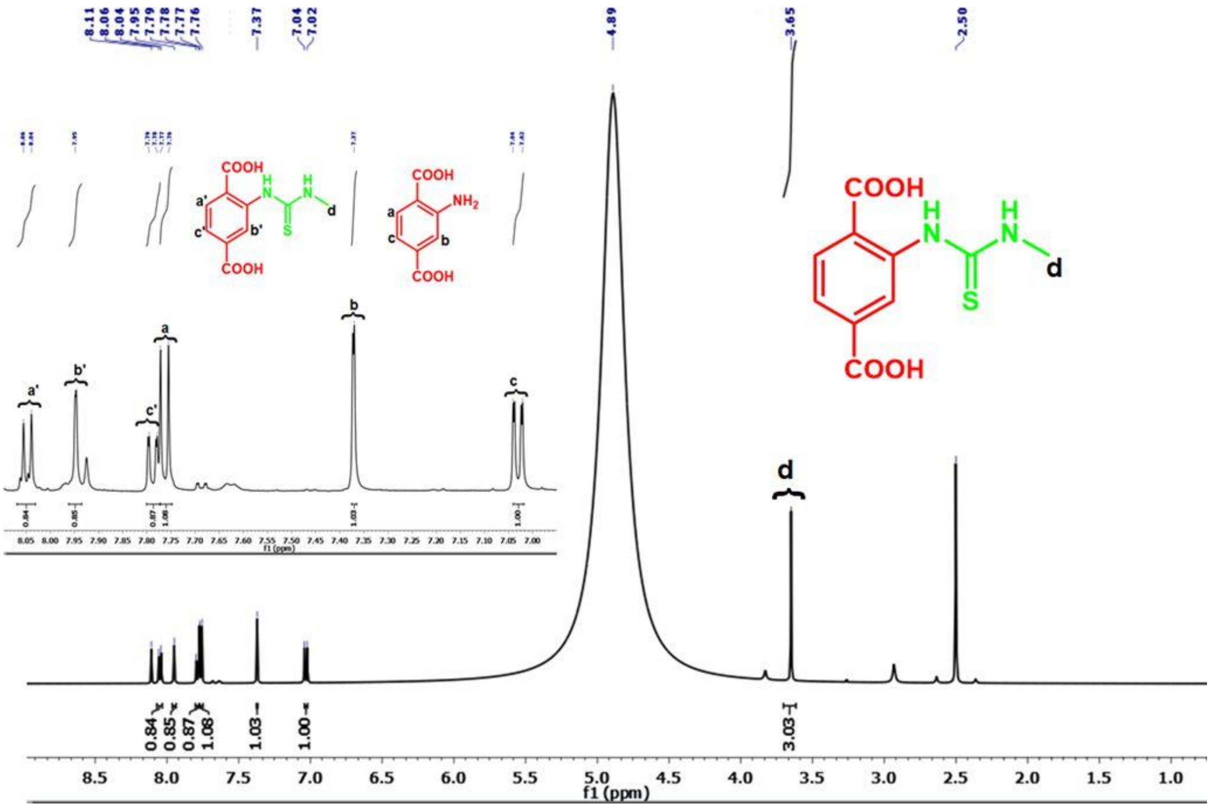

Figure S2. Digested ^{1}H NMR spectrum of **Hf-UiO-66-NHCSNHCH$_3$** MOF (digested using 10 µL of 40% HF in 500 µL of DMSO-D$_6$ and 20 mg of MOF).

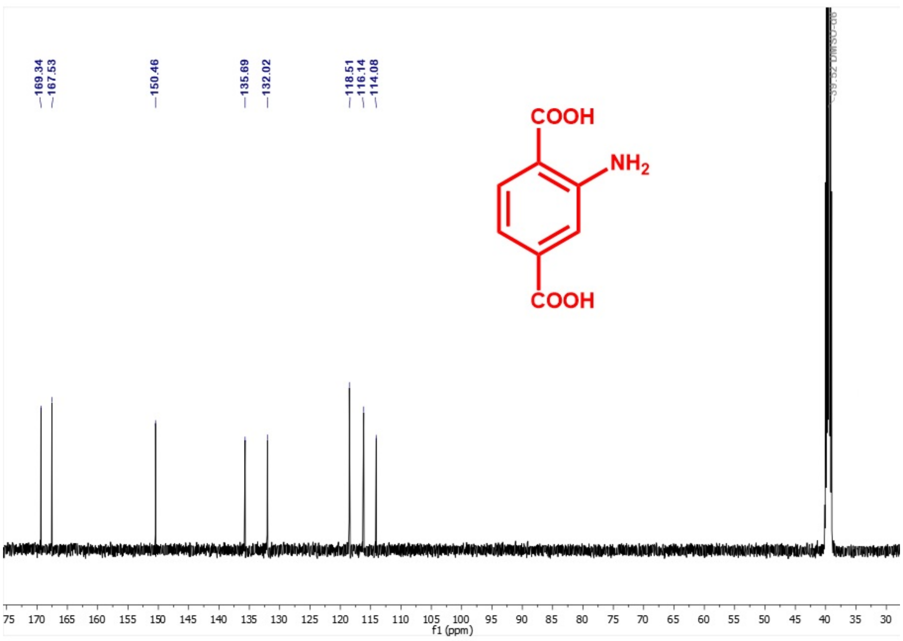

Figure S3. Digested ^{13}C NMR spectrum of **Hf-UiO-66-NH$_2$** (digested using 10 µL of 40% HF in 500 µL of DMSO-D$_6$ and 20 mg of MOF).

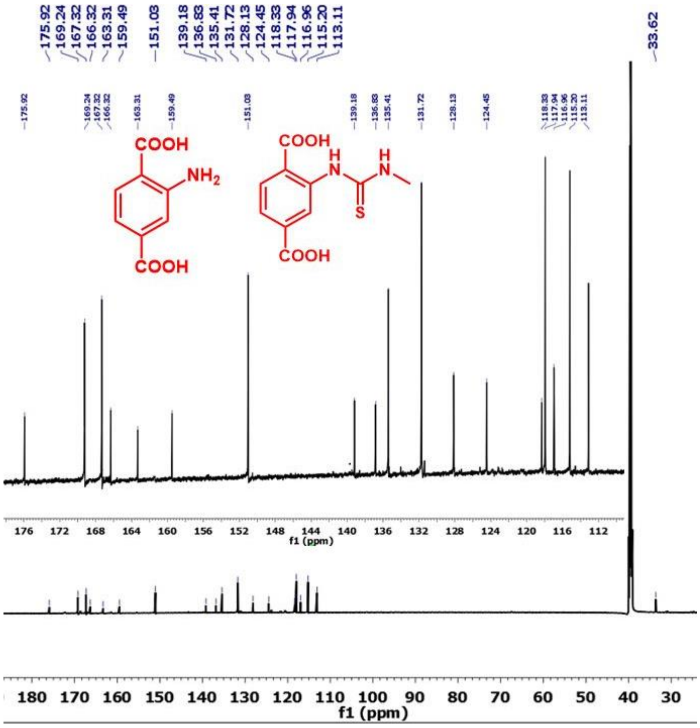

Figure S4. Digested ^{13}C NMR spectrum of **Hf-UiO-66-NHCSNHCH$_3$** MOF (digested using 10 µL of 40% HF in 500 µL of DMSO-D$_6$ and 20 mg of MOF).

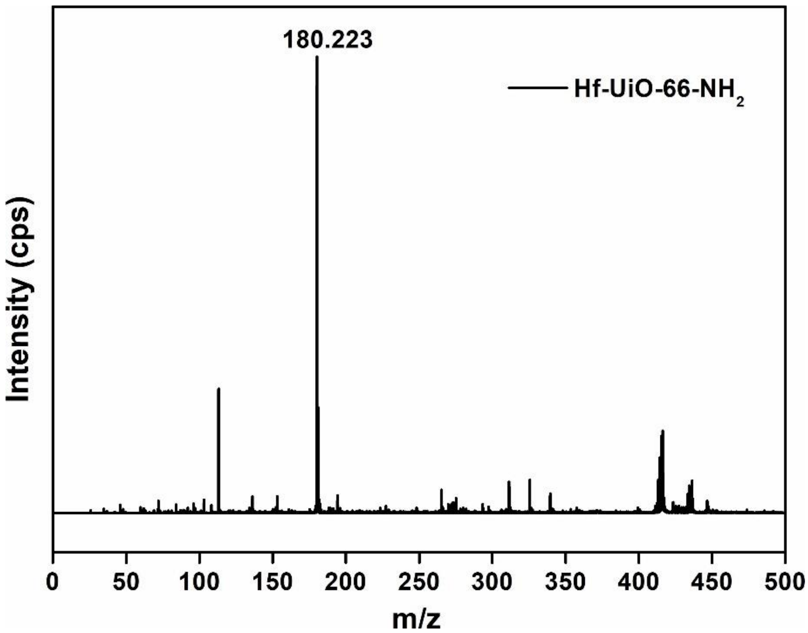

Figure 5. Mass spectrum of **Hf-UiO-66-NH$_2$** after digestion by HF in methanol/water mixture.

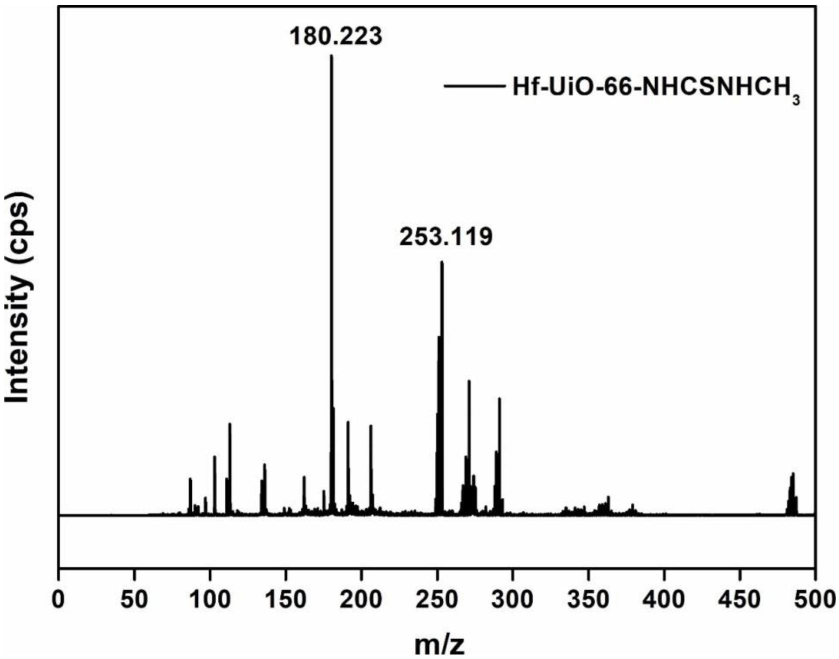

Figure S6. Mass spectrum of **Hf-UiO-66-NHCSNHCH$_3$** after digestion by HF in methanol/water mixture.

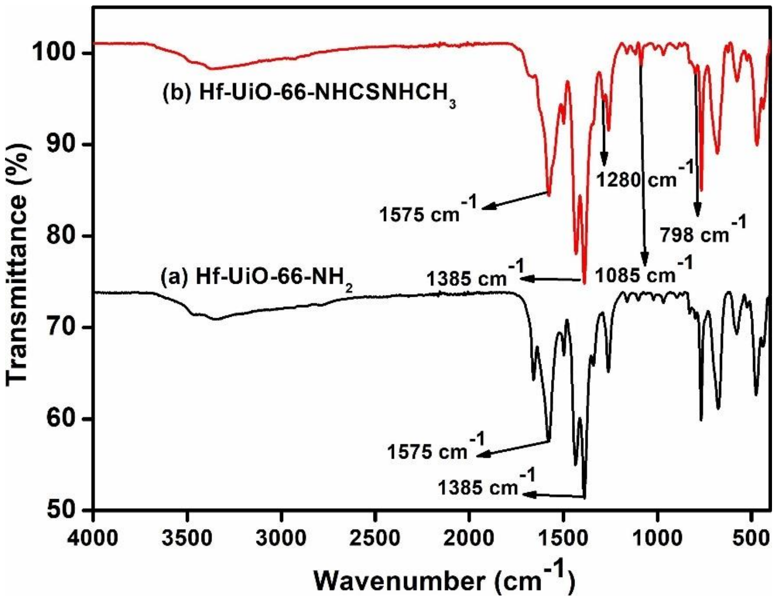

Figure S7. AT-IR spectra of **Hf-UiO-66-NH$_2$** (black) and **Hf-UiO-66-NHCSNHCH$_3$** (red).

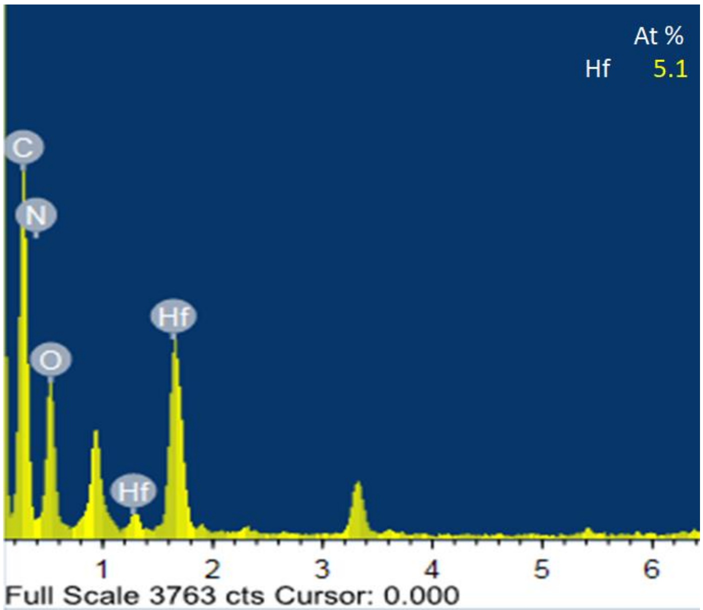

Figure S8. TEM-EDX spectrum of **Hf-UiO-66-NH$_2$**.

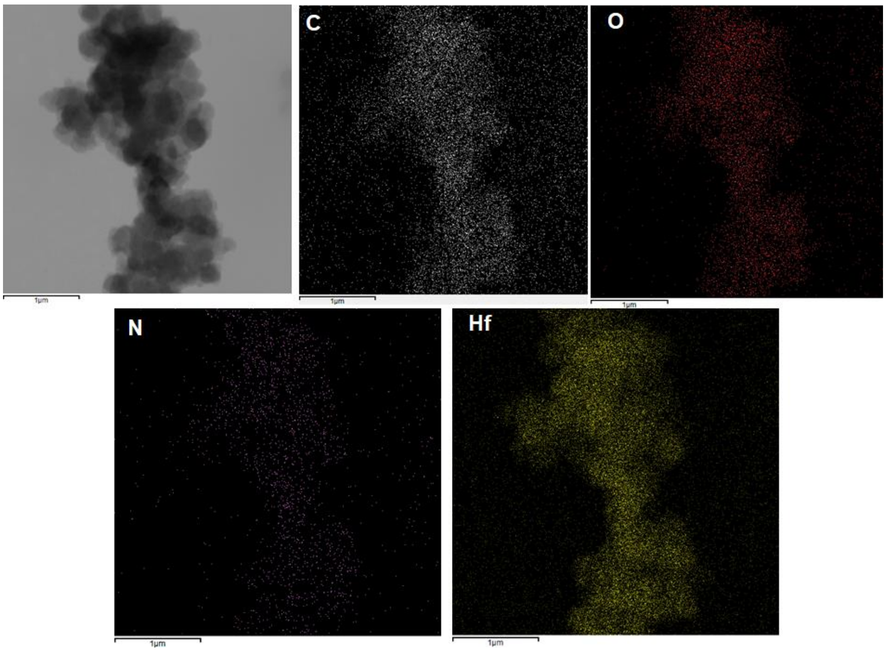

Figure S9. TEM-EDX elemental mapping of **Hf-UiO-66-NH$_2$**.

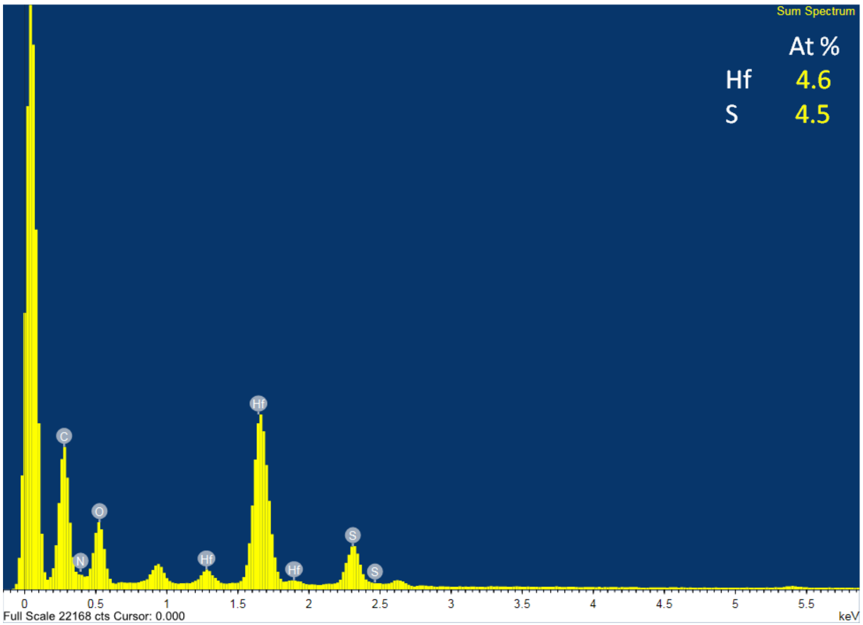

Figure S10. TEM-EDX spectrum of **Hf-UiO-66-NHCSNHCH$_3$**.

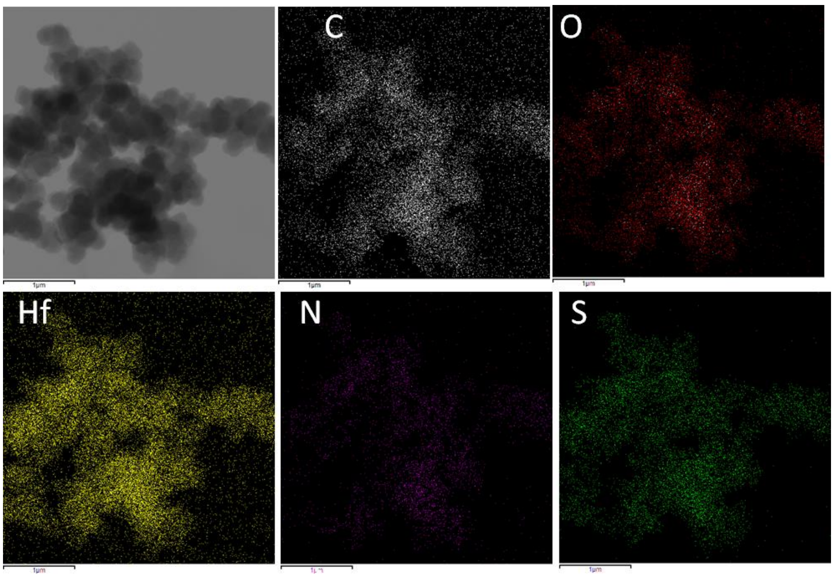

Figure S11. TEM-EDX mapping of **Hf-UiO-66-NHCSNHCH$_3$**.

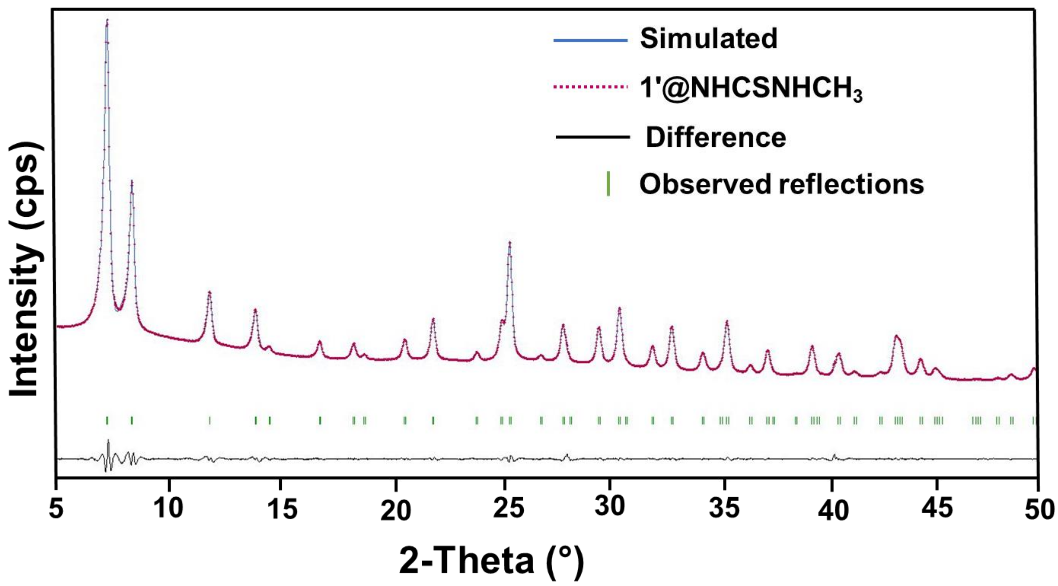

Figure S12. Pawley fit plot for the PXRD pattern of **Hf-UiO-66-NHCSNHCH$_3$** (R_{wp} and R_p are 1.6% and 2.3%, respectively).

Table S1. Indexing parameters of simulated UiO-66 and **Hf-UiO-66-NHCSNHCH3**.

Compound name	$[Hf_6O_4(OH)_4(BDC\text{-}NHCSNHCH_3)_6]\cdot 4H_2O\cdot 5DMF$ (**1**) (this work)	UiO-66 (reported)[1]
Crystal System	Cubic	Cubic
a = b = c (Å)	20.743 (5)	20.700 (2)
α = β= γ (°)	90	90
V (Å^3)	8924.6 (35)	8870.3 (2)
Radiation	Cu Kα1	Cu Kα1

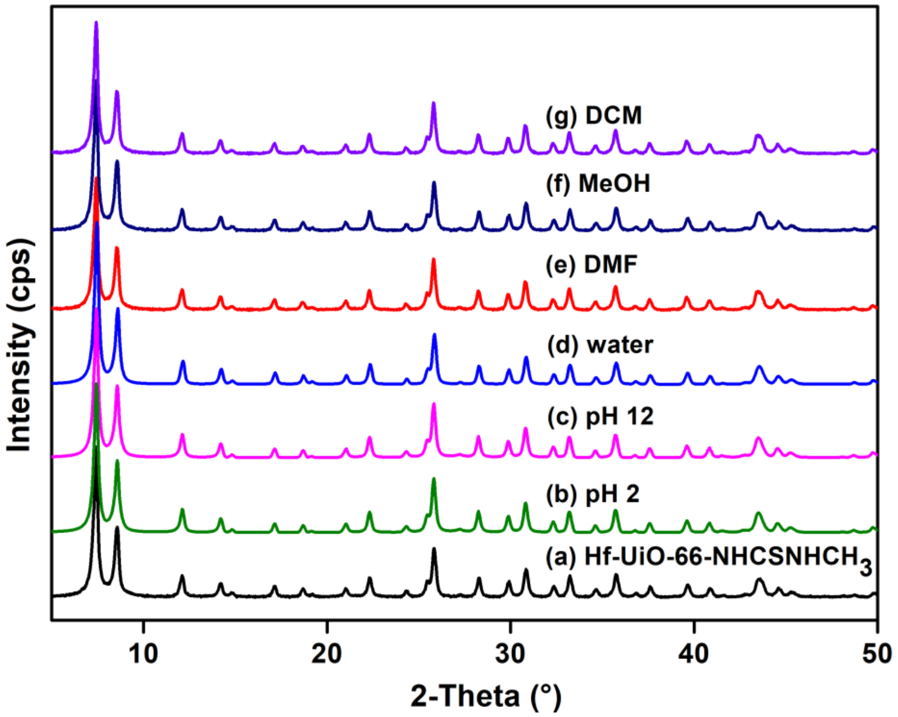

Figure S13. PXRD patterns of **Hf-UiO-66-NHCSNHCH$_3$** (black) and PXRD pattern of the recovered sample after stirring in (b) pH 2 solution (green), (c) pH 12 solution (pink), (d) water (blue), (e) DMF (red), (f) MeOH (deep blue), (g) DCM (violet).

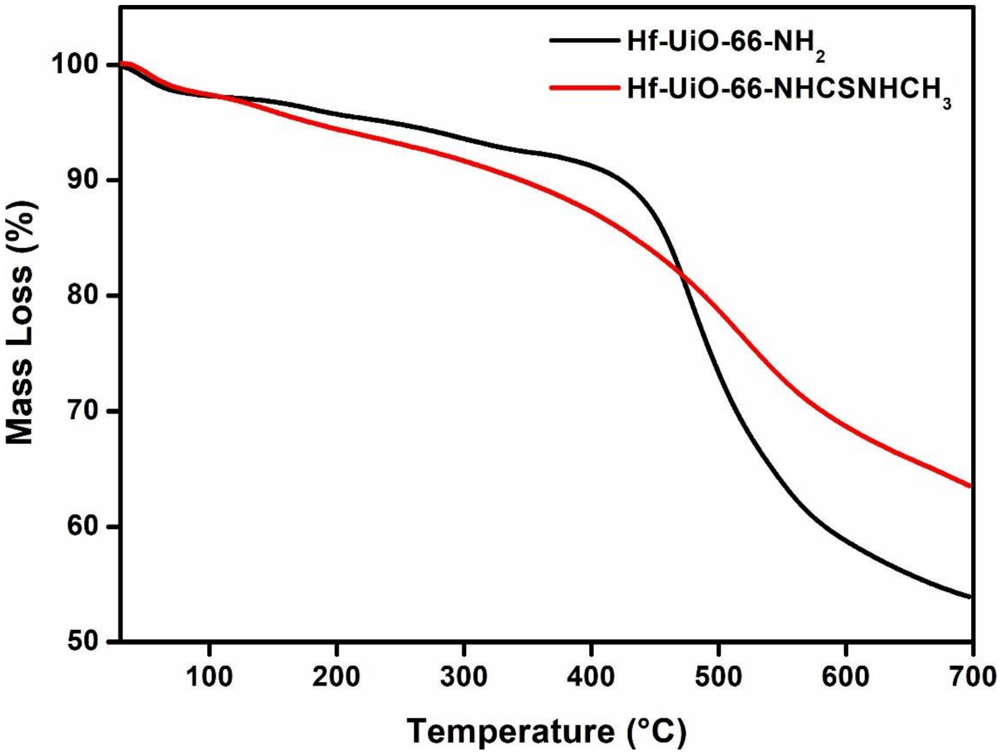

Figure S14. TG curves of **Hf-UiO-66-NHCSNHCH3** and **Hf-UiO-66-NH$_2$** measured at -196 °C.

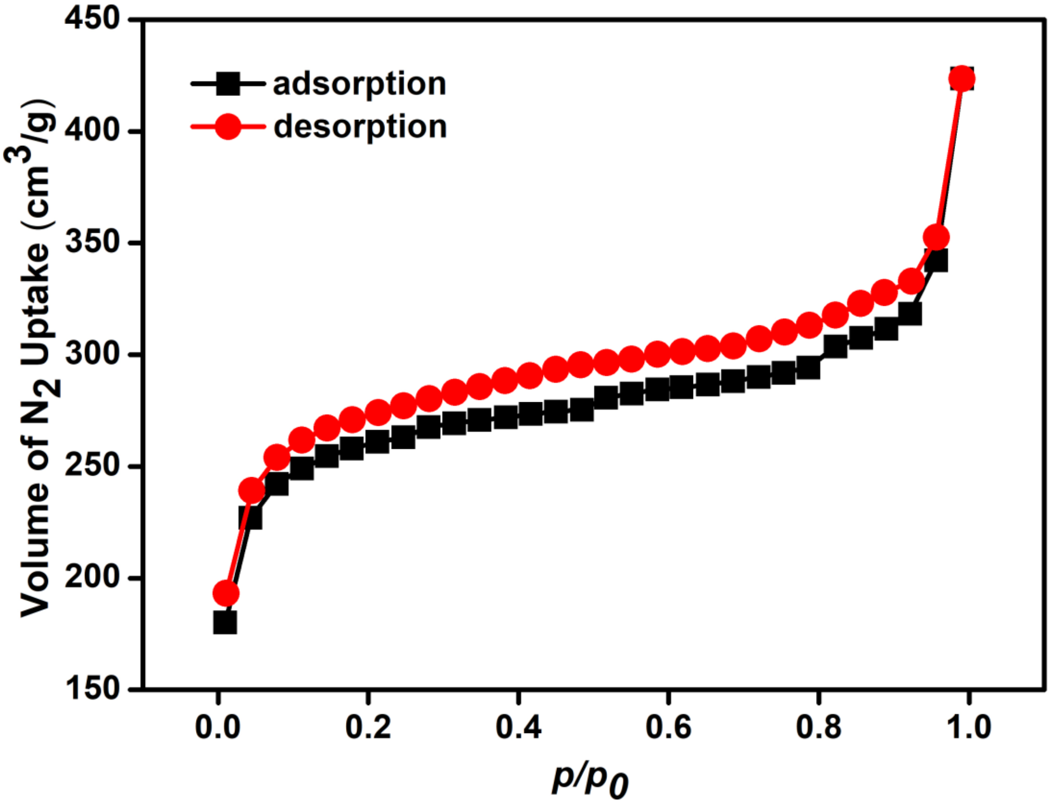

Figure S15. N_2 sorption isotherms of **Hf-UiO-66-NH$_2$** measured at -196 °C.

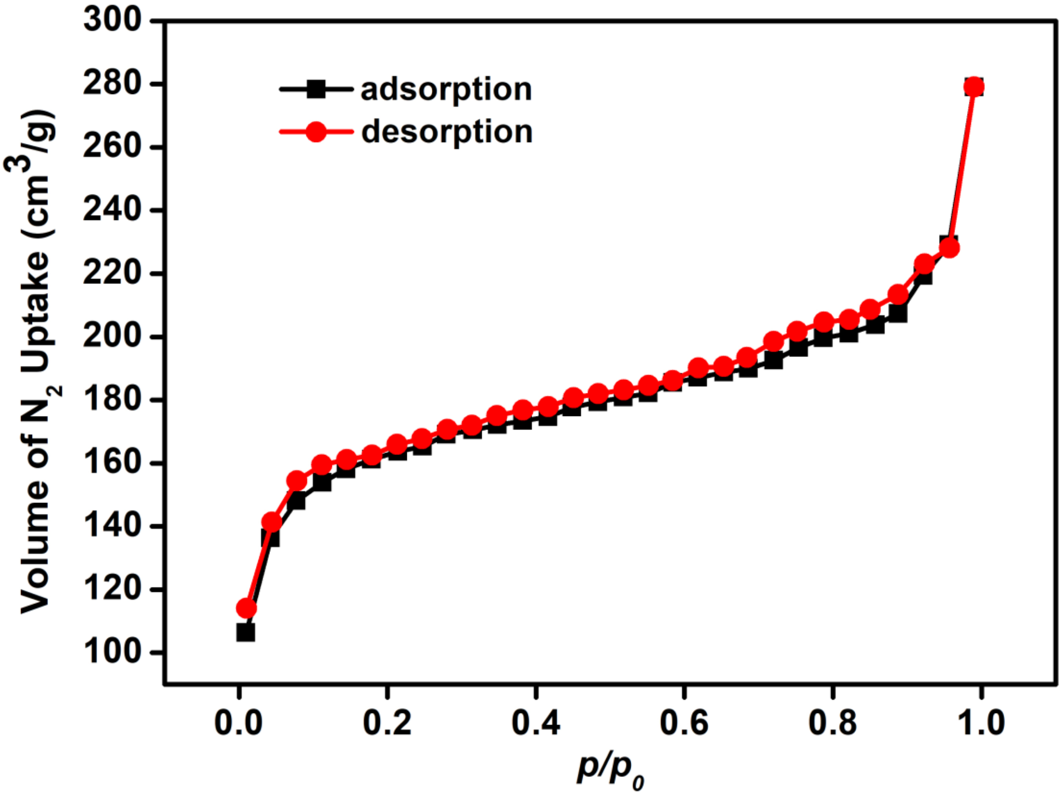

Figure S16. N_2 sorption isotherms of **Hf-UiO-66-NHCSNHCH$_3$** measured at -196 °C.

Table S2. Intra-day and inter-day precession towards detection of Hg^{2+} towards with standard deviation and relative standard deviation.

Volume of Hg^{2+} solution added	Intra-Day Fluorescence Emission Intensity (cps)			Mean (χ)	Standard Deviation (σ)	Relative Standard Deviation (RSD)
0 µL	461358.6	462046.4	461947.9	461784.3	371.9	0.081
50 µL	214541.7	215282.9	216689.2	215504.6	1090.8	0.506
100 µL	124669.3	125729.4	126317.4	125572.0	835.3	0.665
150 µL	77811.0	77153.8	77527.4	77497.4	329.6	0.425
200 µL	48169.6	48736.6	48896.6	48600.9	382.0	0.786
250 µL	33920.7	33296.7	33558.1	33591.8	313.4	0.933
300 µL	22522.4	22841.6	22217.5	22527.1	312.1	1.385
Volume of Hg^{2+} solution added	Inter-Day Fluorescence Emission Intensity (cps)			Mean (χ)	Standard Deviation (σ)	Relative Standard Deviation (RSD)
0 µL	461358.6	462579.4	460047.9	461328.6	1266.0	0.274
50 µL	214541.7	220282.9	218689.7	217837.9	2963.8	1.361
100 µL	124669.3	126532.4	125212.4	125471.4	958.2	0.764
150 µL	77811.0	78039.8	76513.3	77454.7	823.2	1.061
200 µL	48169.6	48254.6	49038.6	48487.6	479.1	0.988
250 µL	33920.7	32485.2	34061.1	33489.0	872.1	2.604
300 µL	22522.4	21832.6	23424.5	22593.2	798.3	3.533

Table S3. Intra-day and inter-day precession towards detection of NH_2-NH_2 with standard deviation and relative standard deviation.

Volume of NH_2-NH_2 Solution Added	Intra-Day Fluorescence Emission Intensity (cps)			Mean (χ)	Standard Deviation (σ)	Relative Standard Deviation (RSD)
0 µL	164150.3	163163.2	163084.1	163465.9	594.1	0.363
50 µL	560246.9	562283.7	563234.3	561921.6	1526.2	0.272
100 µL	1406800.8	1402152.4	1408004.7	1405652.1	3090.1	0.220
150 µL	2516240.9	2513823.7	2508612.3	2512891.8	3898.2	0.155
200 µL	3628730.1	3623210.1	3625432.7	3625790.9	2777.3	0.077
250 µL	4351430.3	4356219.3	4359842.8	4355830.7	4219.8	0.097
300 µL	5075660.6	5084791.6	5078214.6	5079555.4	4711.1	0.093
Volume of NH_2-NH_2 Solution Added	Inter-Day Fluorescence Emission Intensity (cps)			Mean (χ)	Standard Deviation (σ)	Relative Standard Deviation (RSD)
0 µL	164150.3	162578.7	163897.5	163608.8	920.4	0.563
50 µL	560246.9	562237.3	558721.9	560402.04	1762.8	0.315
100 µL	1406800.8	1415758.9	1413975.5	1412178.1	4742.2	0.336

150 µL	2516240.9	2508278.4	2509391.8	2511303.4	4311.3	0.1717
200 µL	3628730.1	3609873.7	3619854.5	3614486.1	5033.2	0.139
250 µL	4351430.3	4360429.6	4349852.3	4353904.0	5706.2	0.1311
300 µL	5075660.6	5100874.7	4997528.2	5058021.0	53884	1.0653

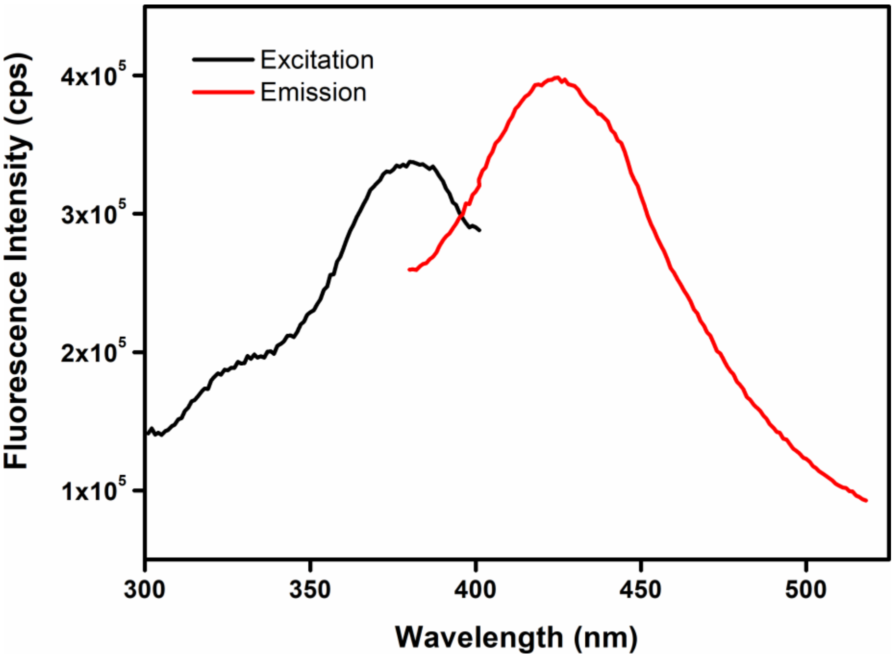

Figure S17. Fluorescence excitation and emission spectra of **Hf-UiO-66-NHCSNHCH$_3$**.

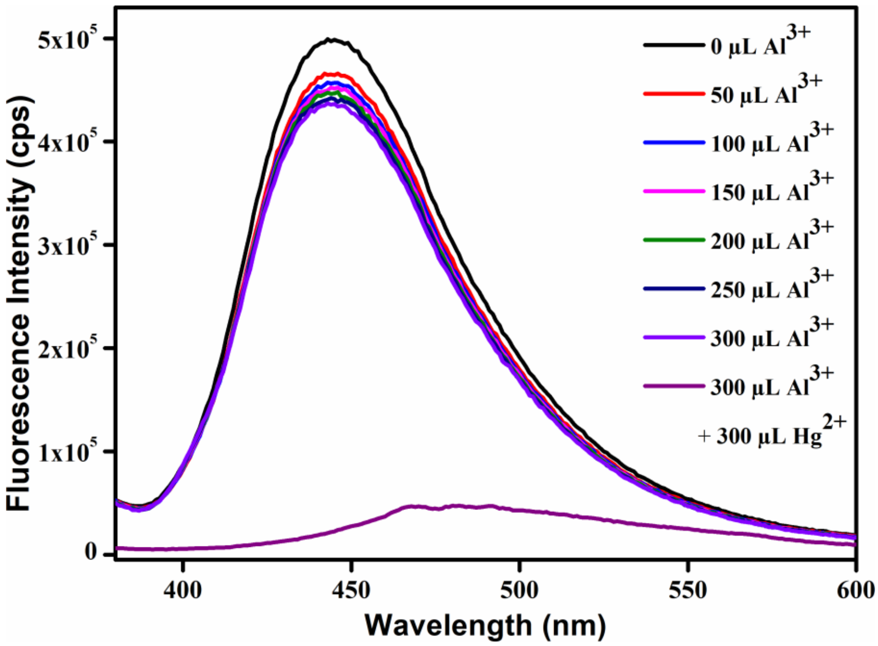

Figure S18. Change in fluorescence emission intensity of probe **Hf-UiO-66-NHCSNHCH$_3$** with the addition of 300 µL of 10 mM aqueous Hg^{2+} solution in the presence of 300 µL of 10 mM aqueous Al^{3+} solution.

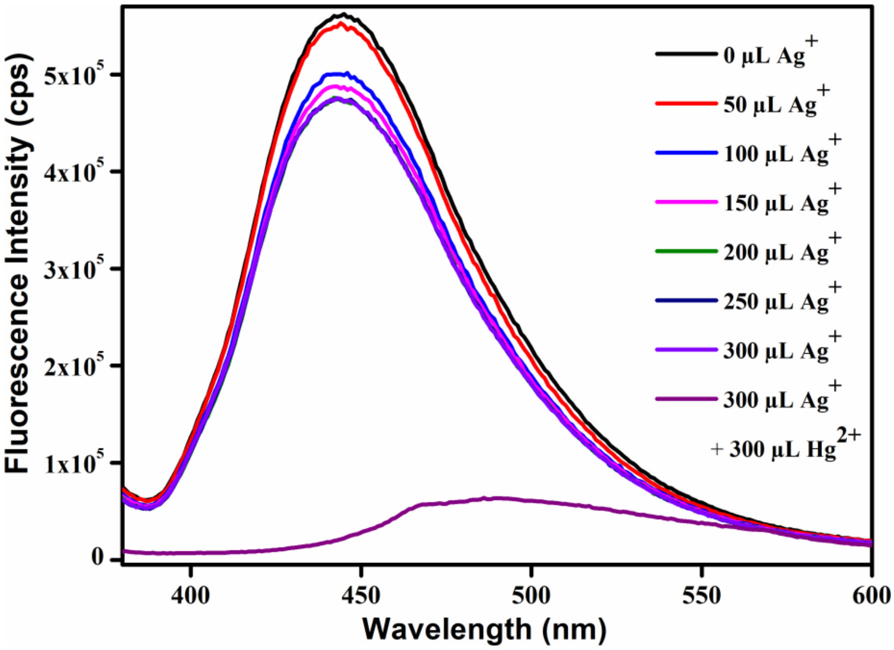

Figure S19. Change in fluorescence emission intensity of probe **Hf-UiO-66-NHCSNHCH$_3$** with the addition of 300 µL of 10 mM aqueous Hg^{2+} solution in the presence of 300 µL of 10 mM aqueous Ag^{+} solution.

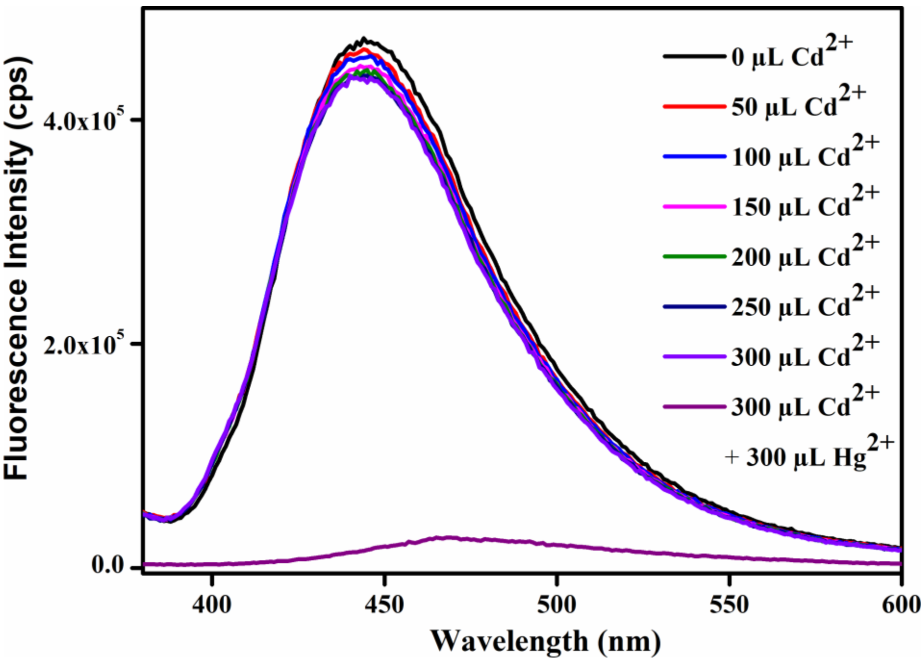

Figure S20. Change in fluorescence emission intensity of probe **Hf-UiO-66-NHCSNHCH$_3$** with the addition of 300 µL of 10 mM aqueous Hg^{2+} solution in the presence of 300 µL of 10 mM aqueous Cd^{2+} solution.

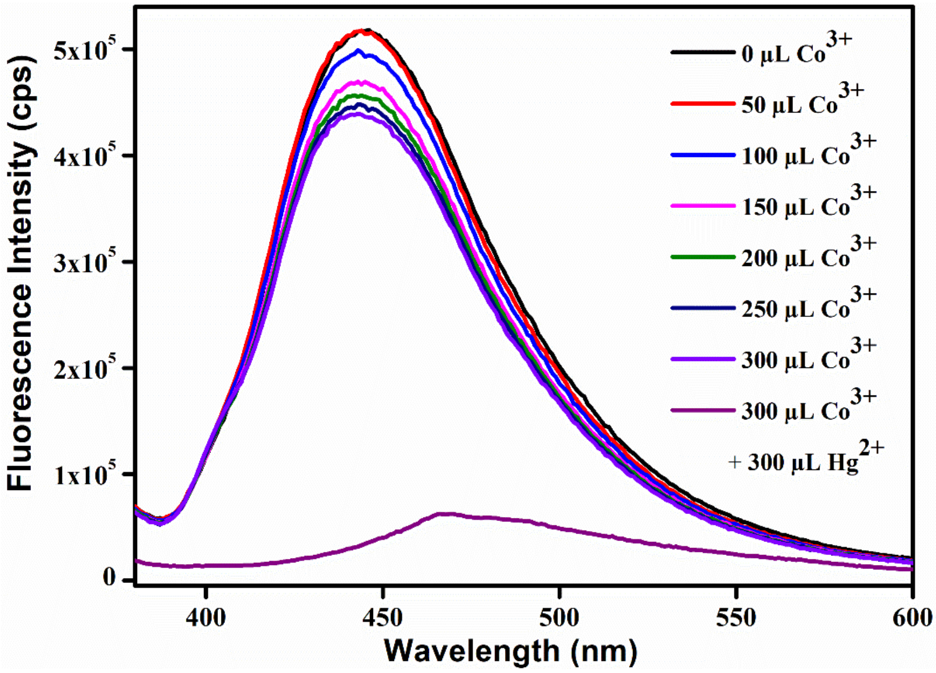

Figure S21. Change in fluorescence emission intensity of probe **Hf-UiO-66-NHCSNHCH$_3$** with the addition of 300 µL of 10 mM aqueous Hg^{2+} solution in the presence of 300 µL of 10 mM aqueous Co^{3+} solution.

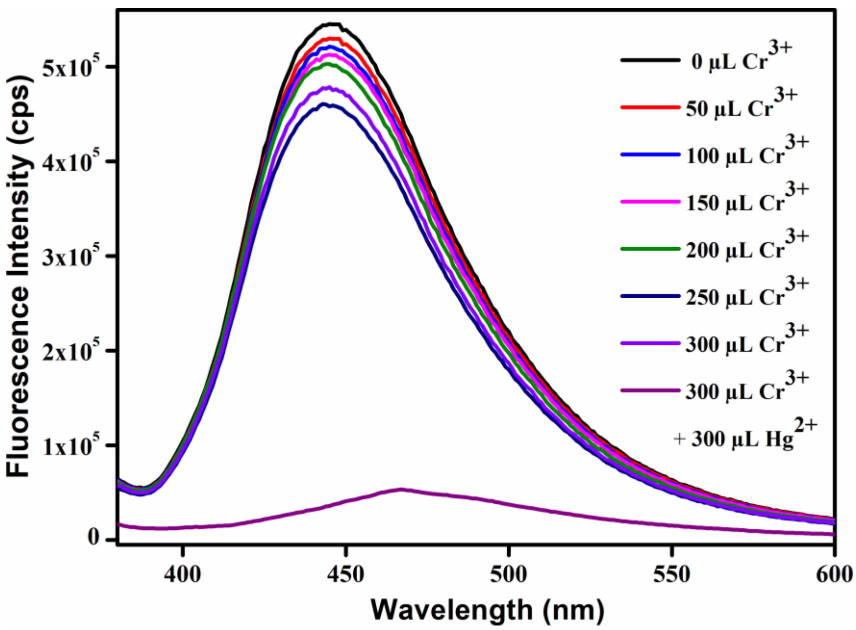

Figure S22. Change in fluorescence emission intensity of probe **Hf-UiO-66-NHCSNHCH$_3$** with the addition of 300 µL of 10 mM aqueous Hg^{2+} solution in the presence of 300 µL of 10 mM aqueous Cr^{3+} solution.

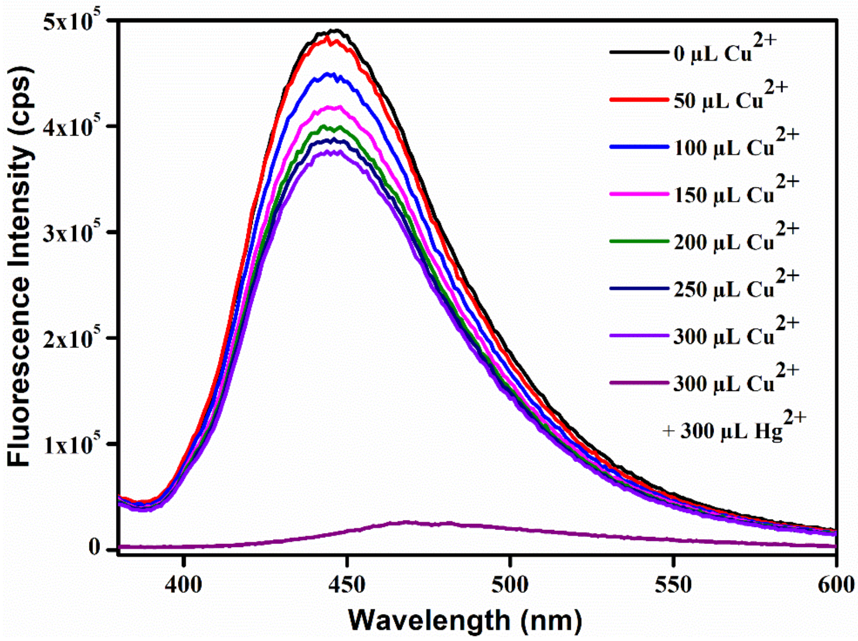

Figure S23. Change in fluorescence emission intensity of probe **Hf-UiO-66-NHCSNHCH$_3$** with the addition of 300 µL of 10 mM aqueous Hg^{2+} solution in the presence of 300 µL of 10 mM aqueous Cu^{2+} solution.

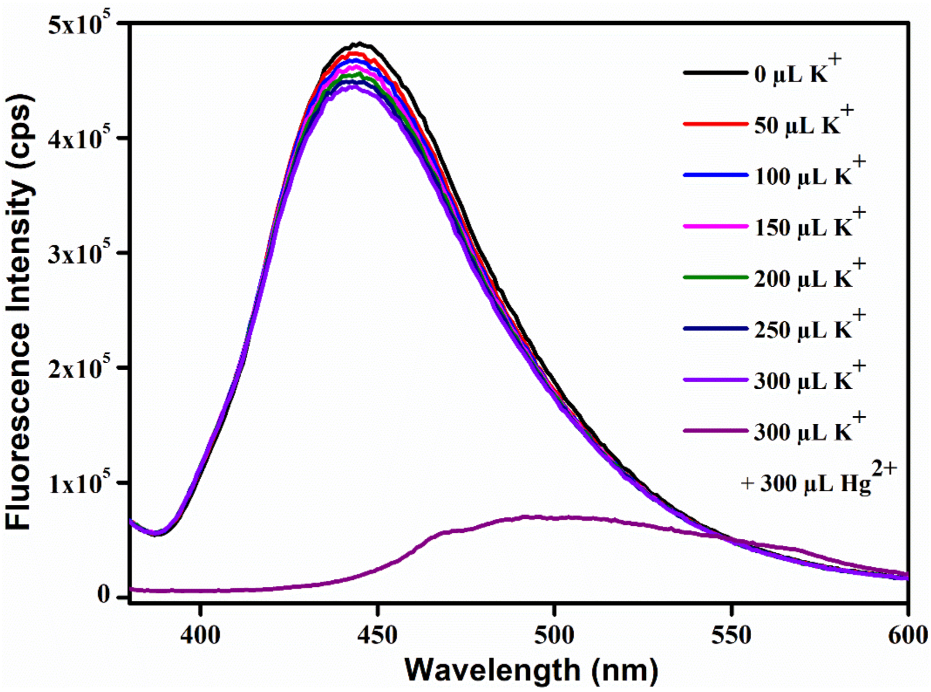

Figure S24. Change in fluorescence emission intensity of probe **Hf-UiO-66-NHCSNHCH$_3$** with the addition of 300 µL of 10 mM aqueous Hg^{2+} solution in the presence of 300 µL of 10 mM aqueous K^{+} solution.

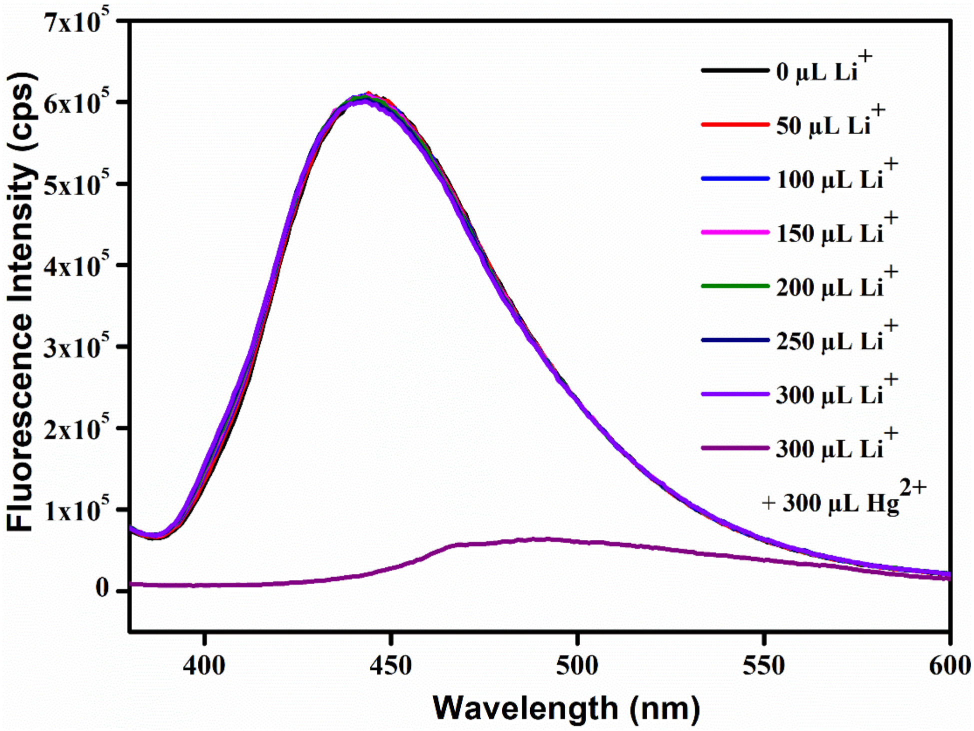

Figure S25. Change in fluorescence emission intensity of probe **Hf-UiO-66-NHCSNHCH$_3$** with the addition of 300 μL of 10 mM aqueous Hg^{2+} solution in the presence of 300 μL of 10 mM aqueous Li^{+} solution.

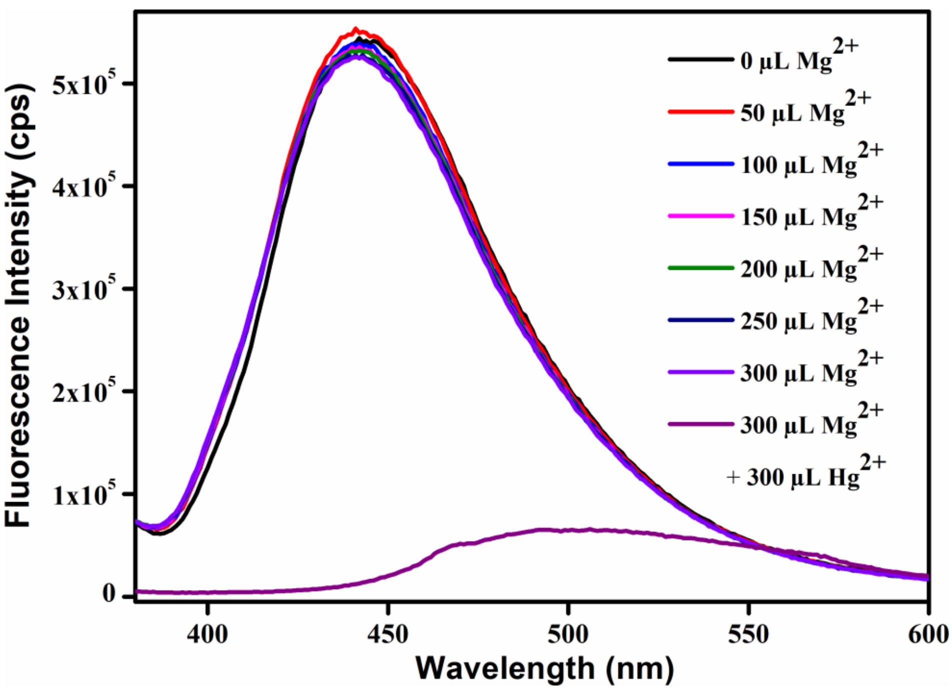

Figure S26. Change in fluorescence emission intensity of probe **Hf-UiO-66-NHCSNHCH$_3$** with the addition of 300 μL of 10 mM aqueous Hg^{2+} solution in the presence of 300 μL of 10 mM aqueous Mg^{2+} solution.

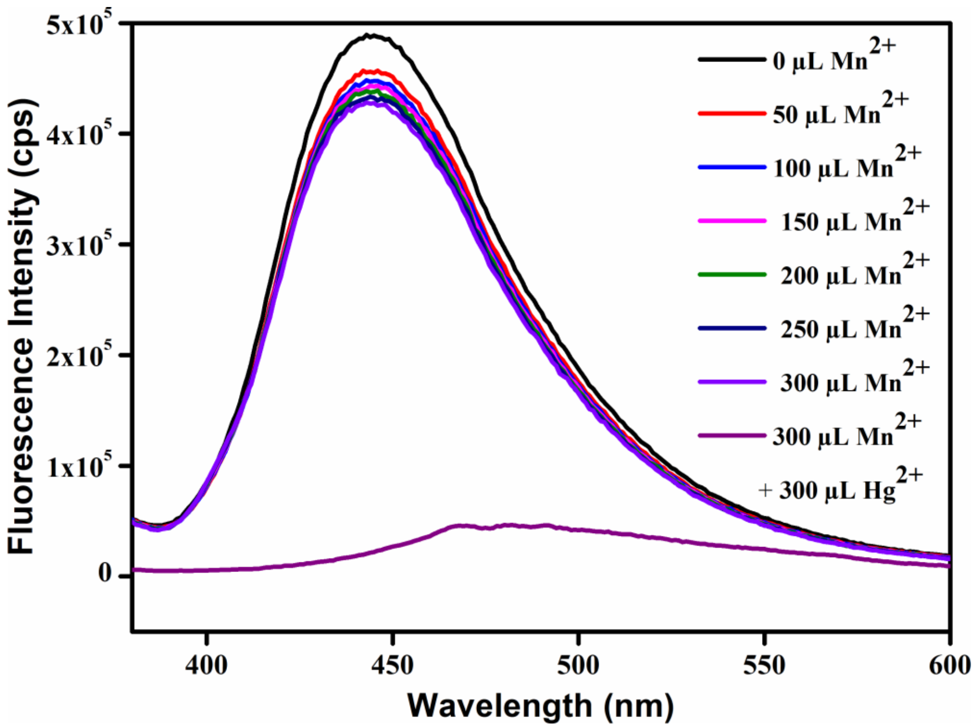

Figure S27. Change in fluorescence emission intensity of probe **Hf-UiO-66-NHCSNHCH$_3$** with the addition of 300 µL of 10 mM aqueous Hg^{2+} solution in the presence of 300 µL of 10 mM aqueous Mn^{2+} solution.

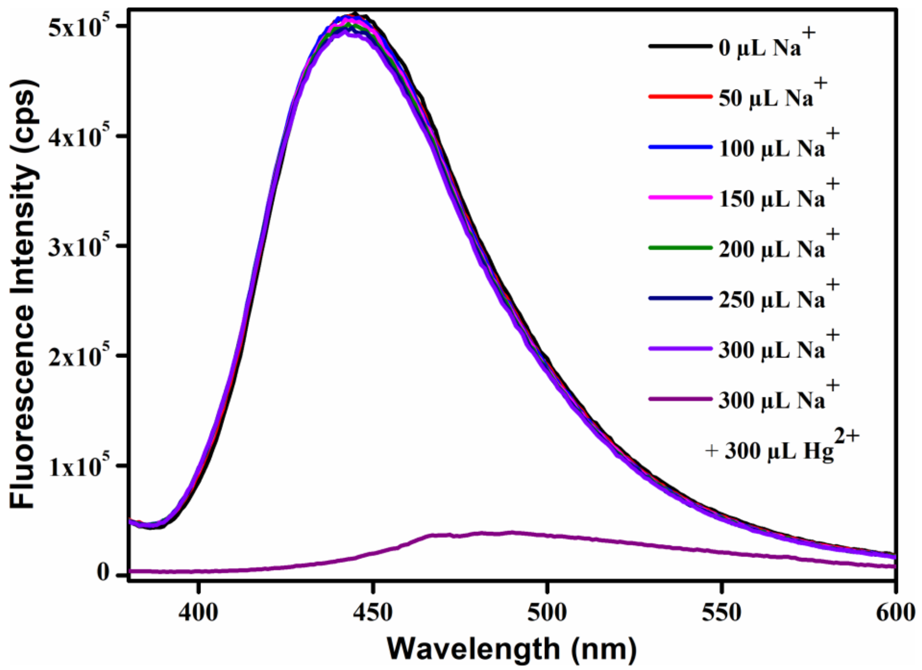

Figure S28. Change in fluorescence emission intensity of probe **Hf-UiO-66-NHCSNHCH$_3$** with the addition of 300 µL of 10 mM aqueous Hg^{2+} solution in the presence of 300 µL of 10 mM aqueous Na^{+} solution.

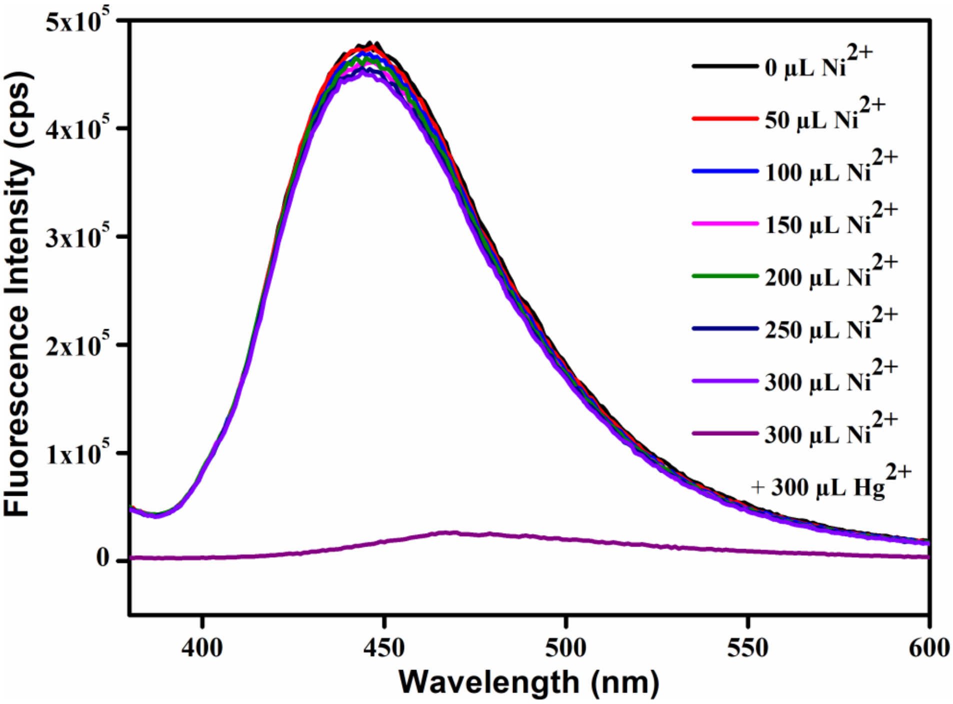

Figure S29. Change in fluorescence emission intensity of probe **Hf-UiO-66-NHCSNHCH$_3$** with the addition of 300 µL of 10 mM aqueous Hg^{2+} solution in the presence of 300 µL of 10 mM aqueous Ni^{2+} solution.

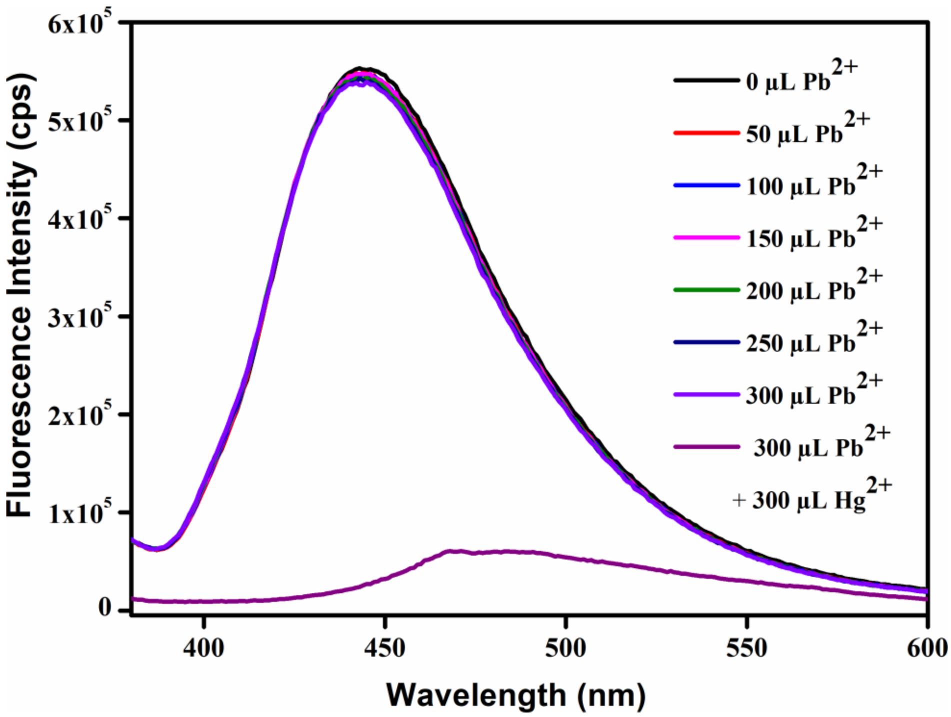

Figure S30. Change in fluorescence emission intensity of probe **Hf-UiO-66-NHCSNHCH$_3$** with the addition of 300 µL of 10 mM aqueous Hg^{2+} solution in the presence of 300 µL of 10 mM aqueous Pb^{2+} solution.

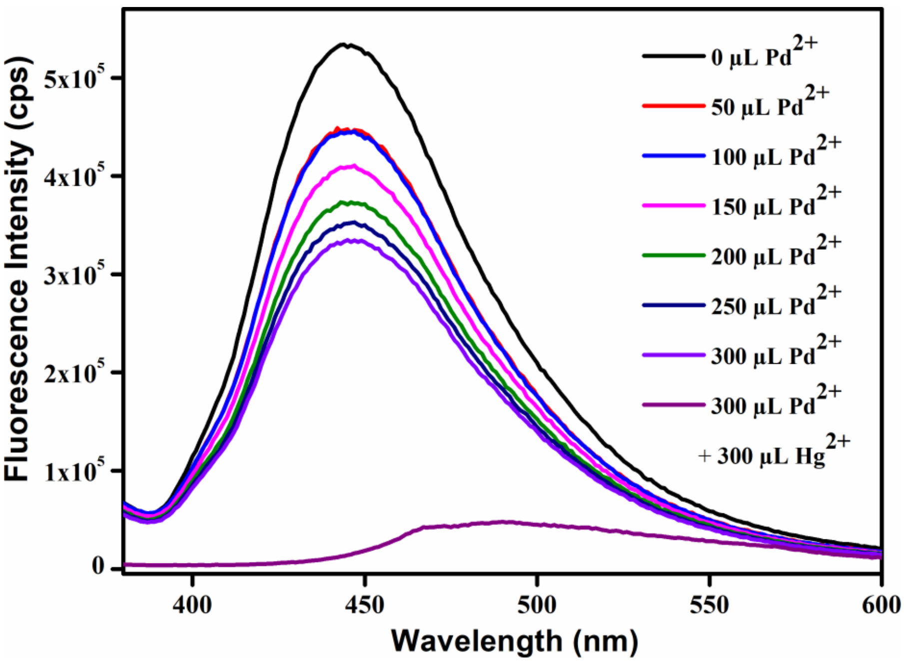

Figure S31. Change in fluorescence emission intensity of probe **Hf-UiO-66-NHCSNHCH$_3$** with the addition of 300 µL of 10 mM aqueous Hg^{2+} solution in the presence of 300 µL of 10 mM aqueous Pd^{2+} solution.

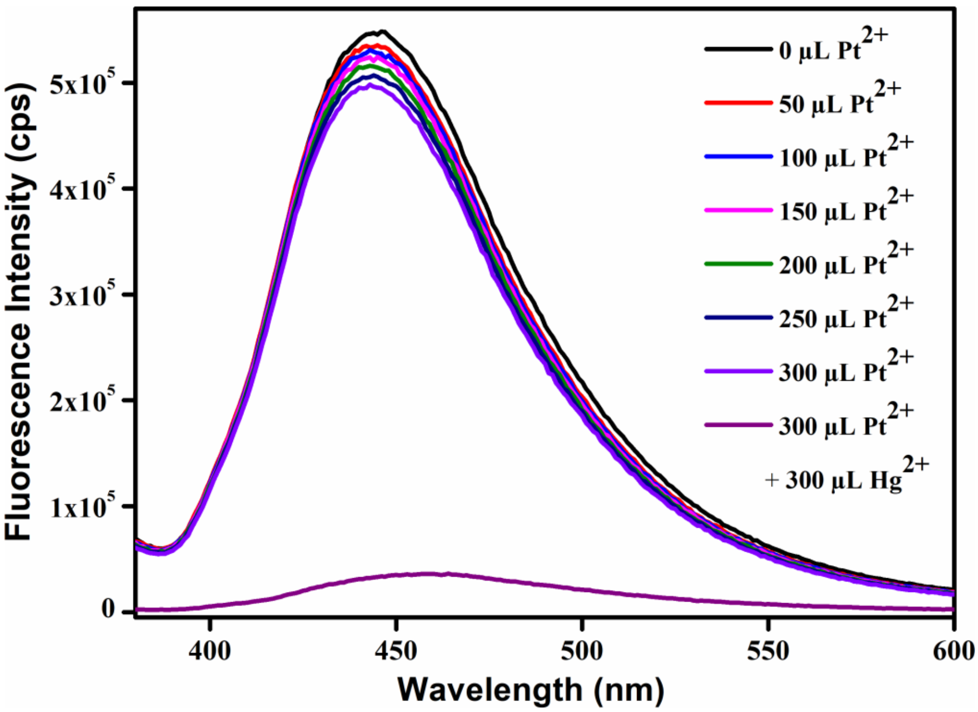

Figure S32. Change in fluorescence emission intensity of probe **Hf-UiO-66-NHCSNHCH$_3$** with the addition of 300 µL of 10 mM aqueous Hg^{2+} solution in the presence of 300 µL of 10 mM aqueous Pt^{2+} solution.

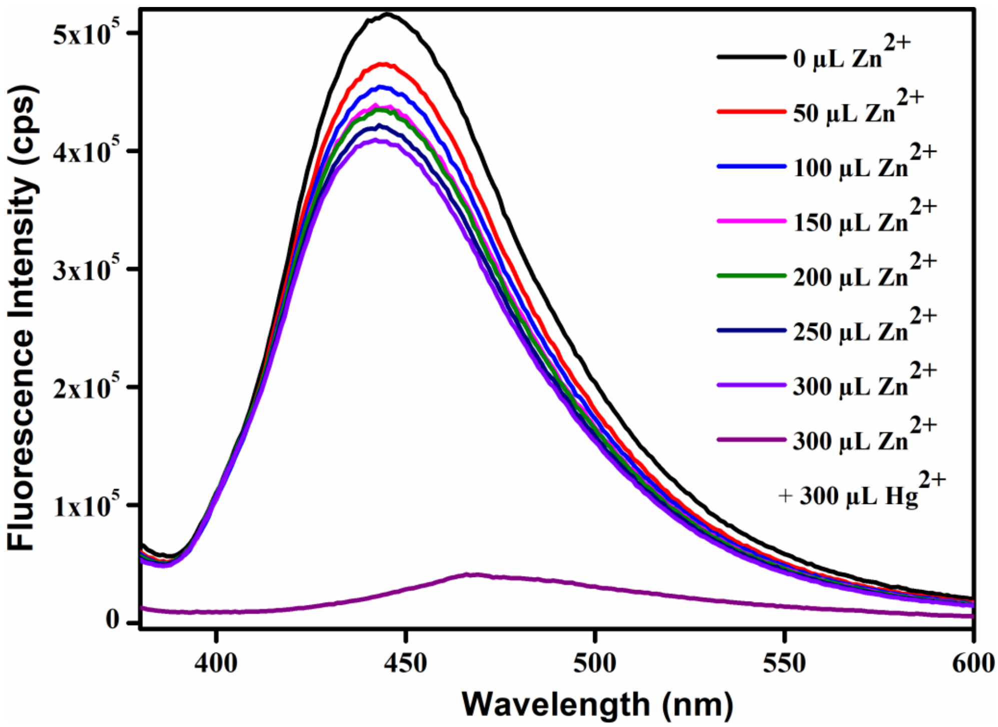

Figure S33. Change in fluorescence emission intensity of probe **Hf-UiO-66-NHCSNHCH$_3$** with the addition of 300 µL of 10 mM aqueous Hg^{2+} solution in the presence of 300 µL of 10 mM aqueous Zn^{2+} solution.

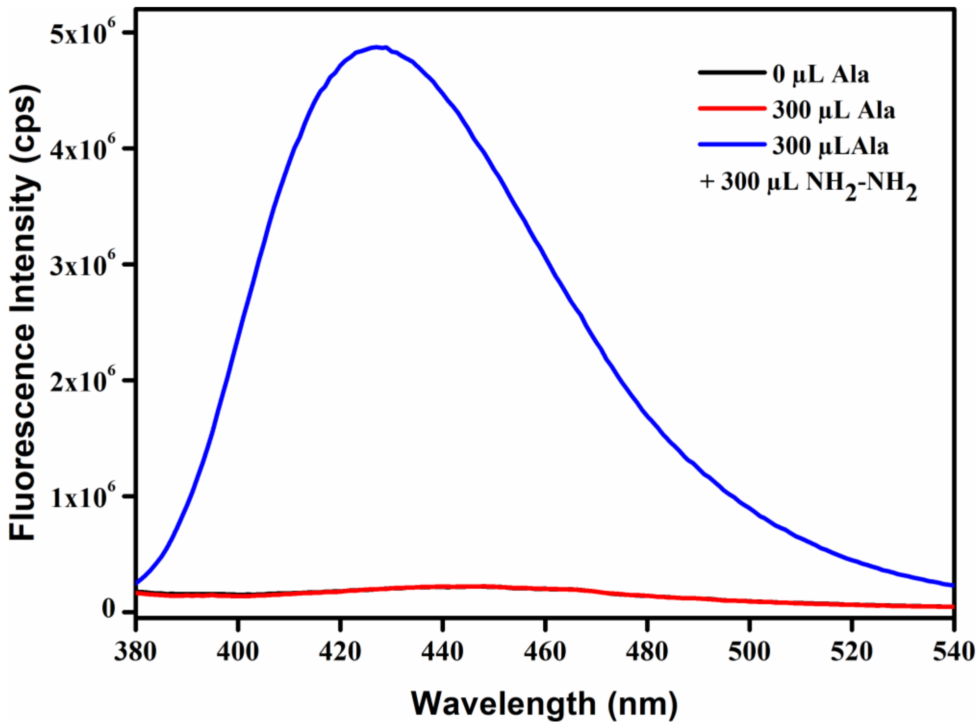

Figure S34. Change in fluorescence emission intensity of probe **Hf-UiO-66-NHCSNHCH$_3$** with the addition of 300 µL of 10 mM aqueous hydrazine solution in the presence of 300 µL of 10 mM aqueous alanine solution.

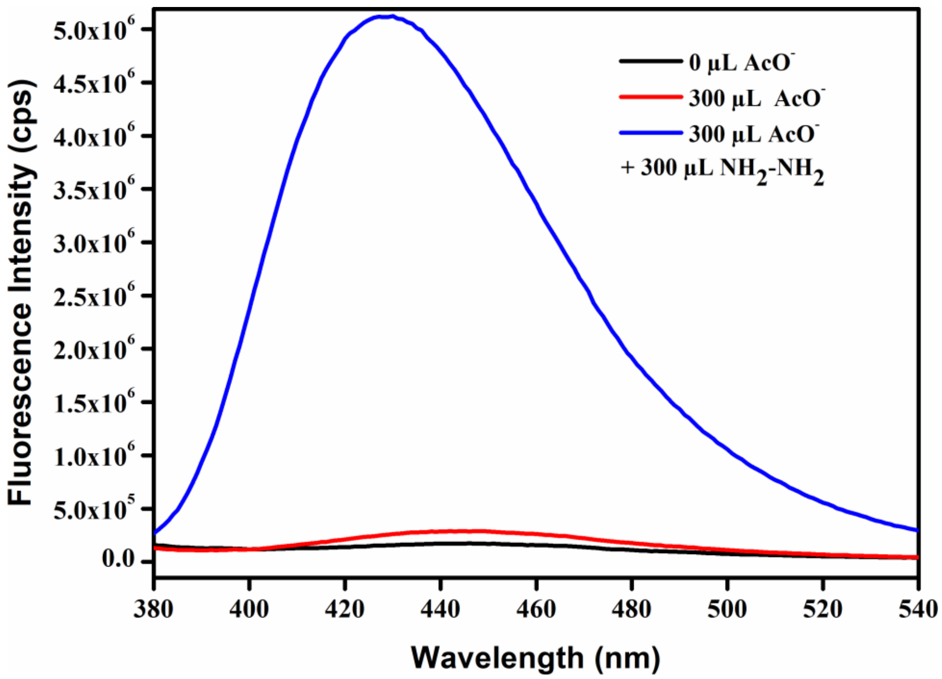

Figure S35. Change in fluorescence emission intensity of probe **Hf-UiO-66-NHCSNHCH$_3$** with the addition of 300 µL of 10 mM aqueous hydrazine solution in the presence of 300 µL of 10 mM aqueous CH_3COO^- solution.

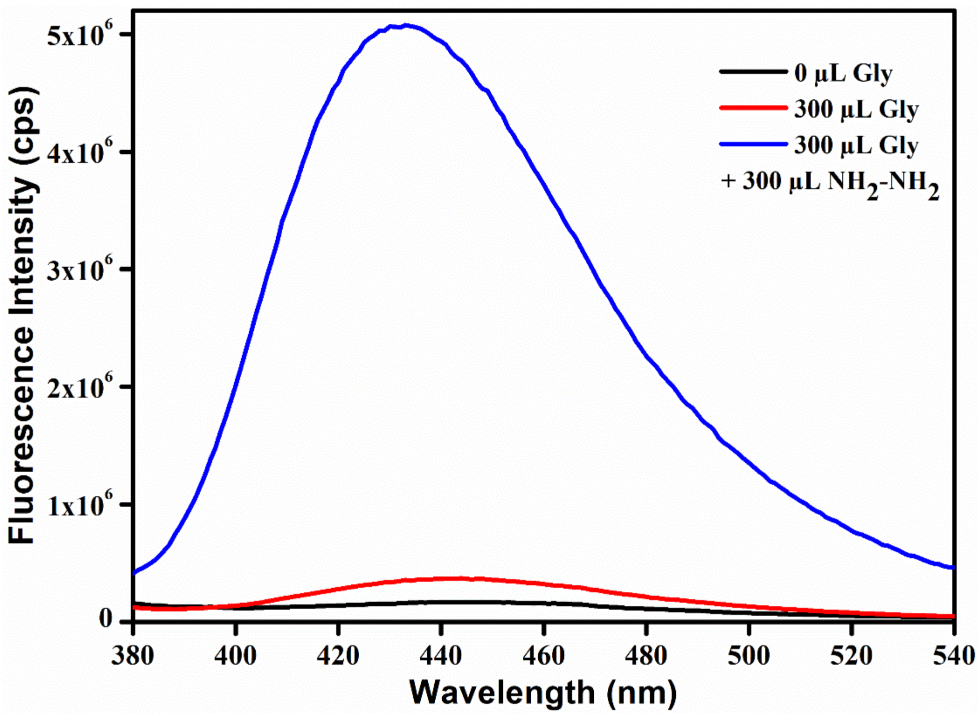

Figure S36. Change in fluorescence emission intensity of probe **Hf-UiO-66-NHCSNHCH$_3$** with the addition of 300 µL of 10 mM aqueous hydrazine solution in the presence of 300 µL of 10 mM aqueous glycine solution.

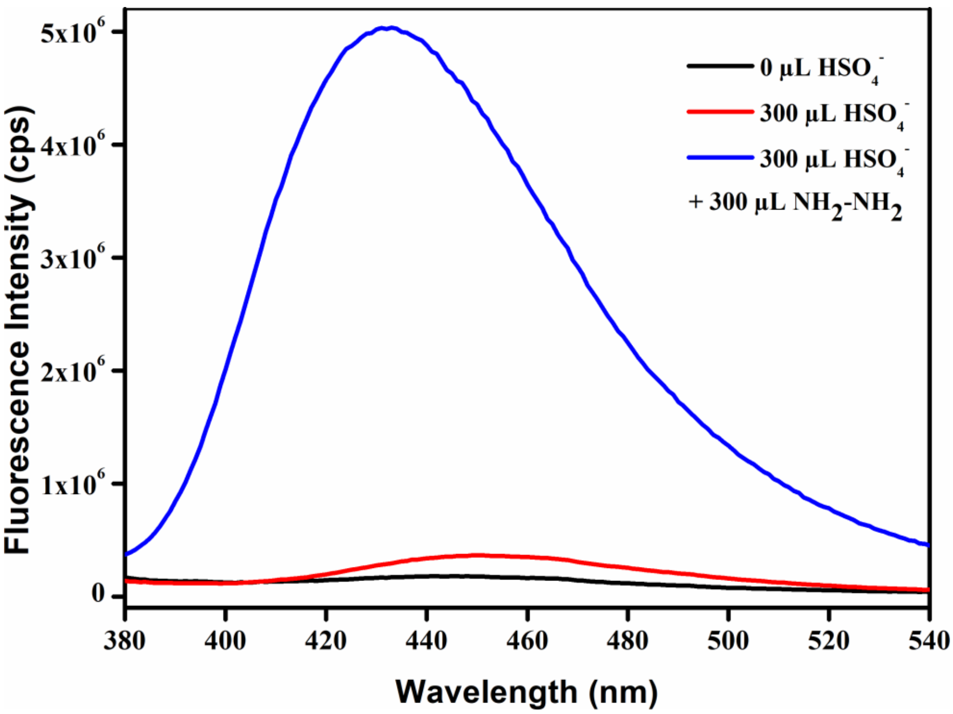

Figure S37. Change in fluorescence emission intensity of probe **Hf-UiO-66-NHCSNHCH$_3$** with the addition of 300 µL of 10 mM aqueous hydrazine solution in the presence of 300 µL of 10 mM aqueous HSO_4^- solution.

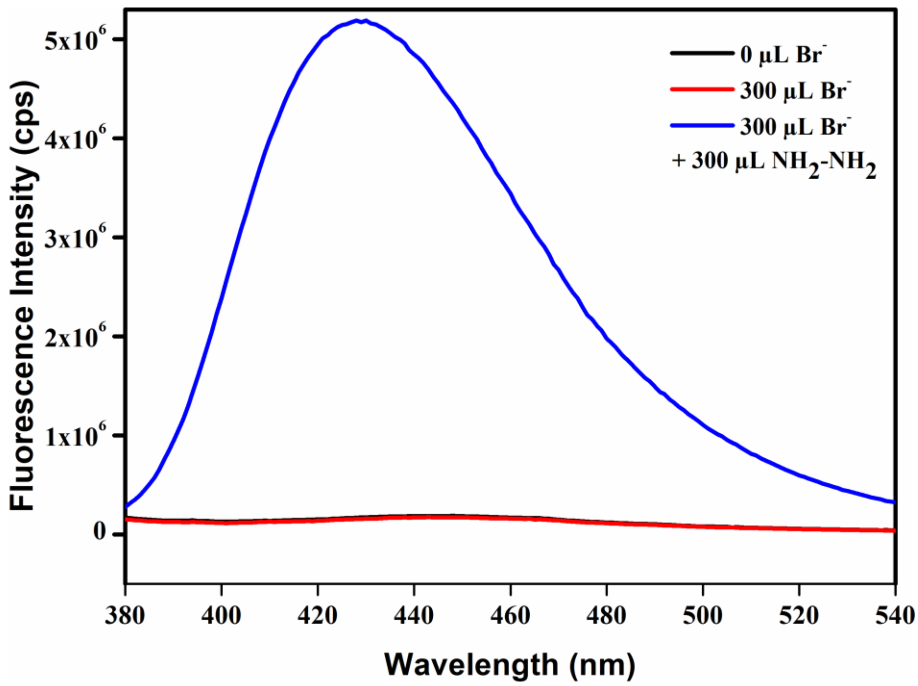

Figure S38. Change in fluorescence emission intensity of probe **Hf-UiO-66-NHCSNHCH$_3$** with the addition of 300 µL of 10 mM aqueous hydrazine solution in the presence of 300 µL of 10 mM aqueous Br^- solution.

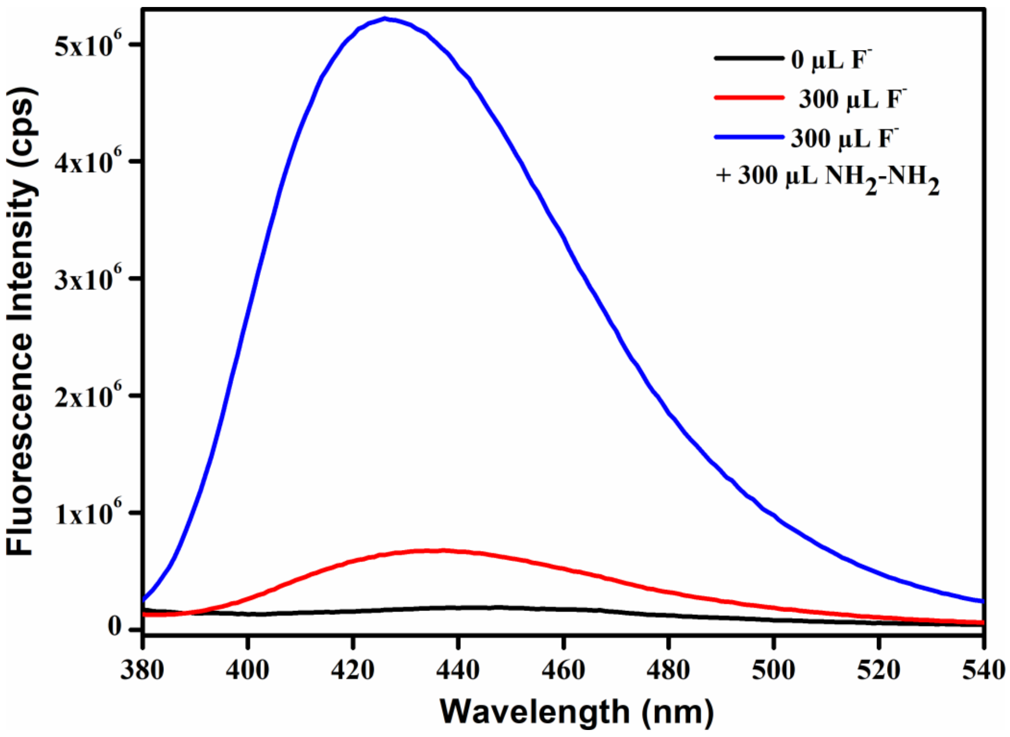

Figure S39. Change in fluorescence emission intensity of probe **Hf-UiO-66-NHCSNHCH$_3$** with the addition of 300 µL of 10 mM aqueous hydrazine solution in the presence of 300 µL of 10 mM aqueous F^- solution.

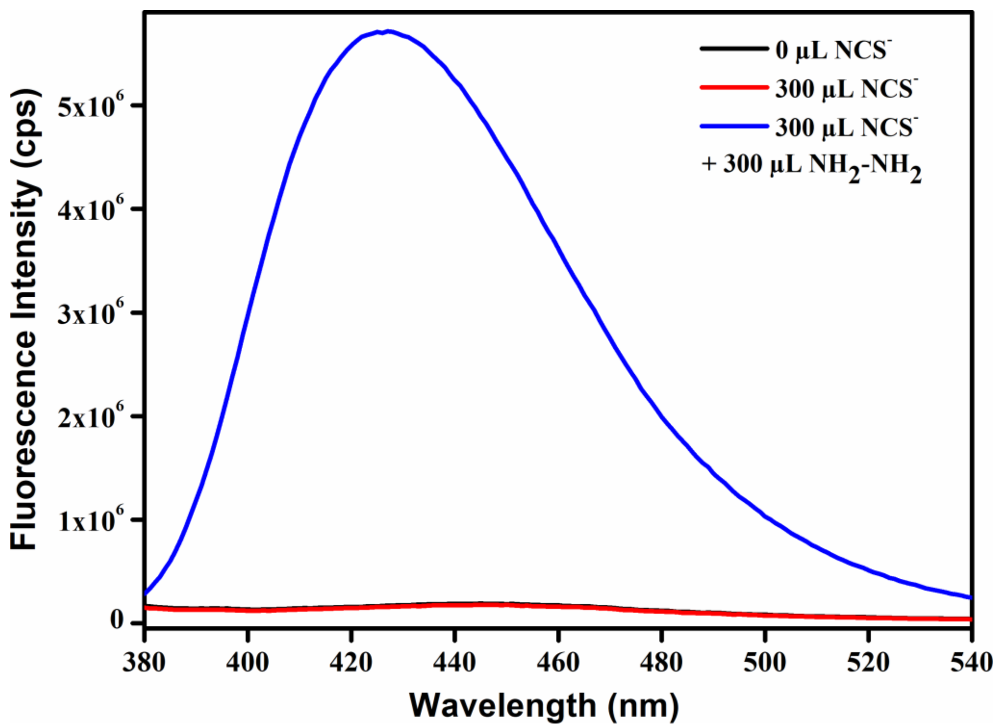

Figure S40. Change in fluorescence emission intensity of probe **Hf-UiO-66-NHCSNHCH$_3$** with the addition of 300 µL of 10 mM aqueous hydrazine solution in the presence of 300 µL of 10 mM aqueous NCS^- solution.

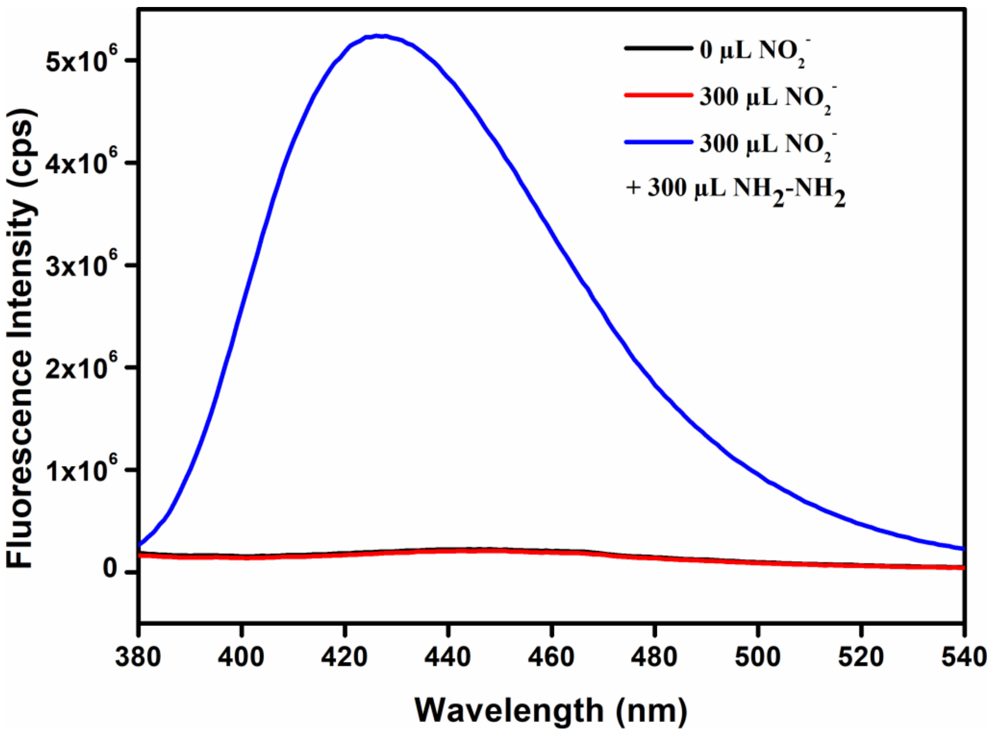

Figure S41. Change in fluorescence emission intensity of probe **Hf-UiO-66-NHCSNHCH$_3$** with the addition of 300 µL of 10 mM aqueous hydrazine solution in the presence of 300 µL of 10 mM aqueous NO_2^- solution.

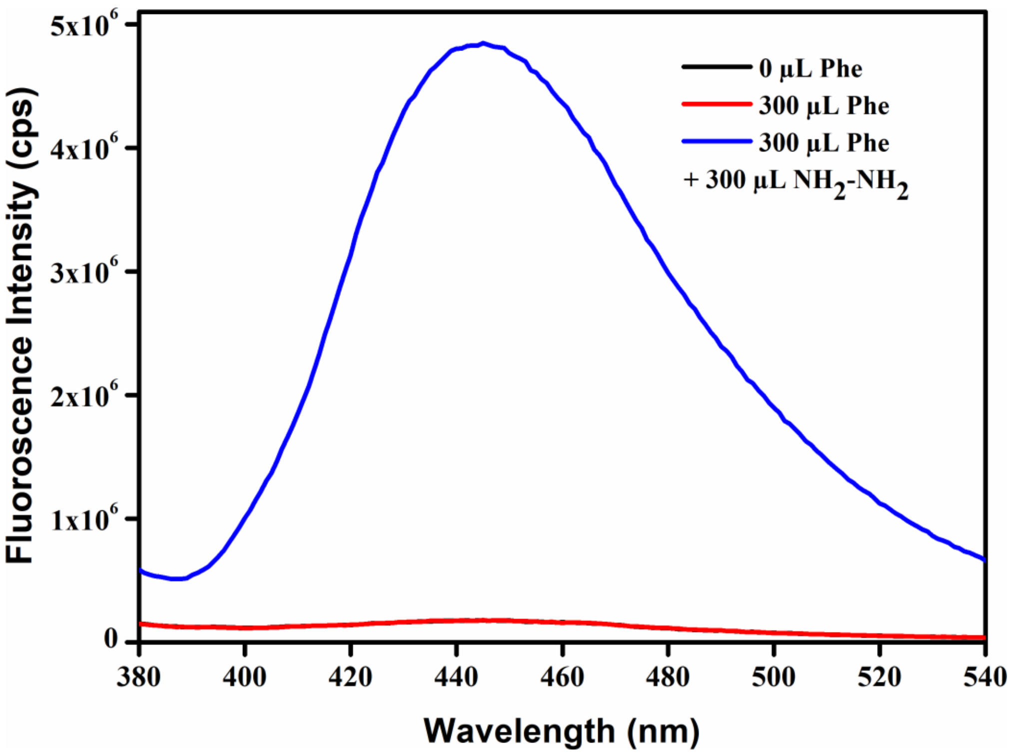

Figure S42. Change in fluorescence emission intensity of probe **Hf-UiO-66-NHCSNHCH$_3$** with the addition of 300 µL of 10 mM aqueous hydrazine solution in the presence of 300 µL of 10 mM aqueous phenyl alanine solution.

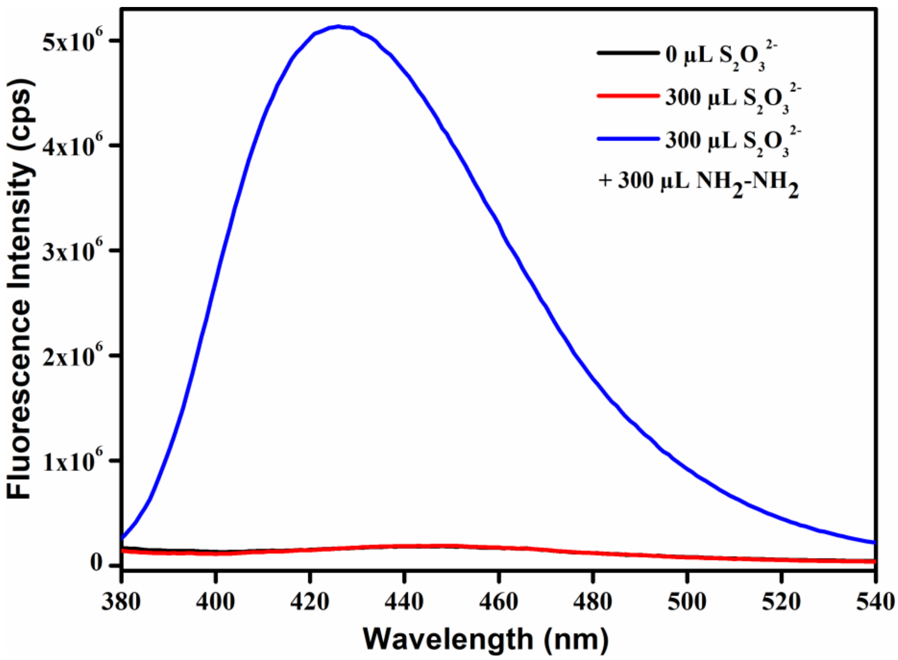

Figure S43. Change in fluorescence emission intensity of probe **Hf-UiO-66-NHCSNHCH$_3$** with the addition of 300 µL of 10 mM aqueous hydrazine solution in the presence of 300 µL of 10 mM aqueous $S_2O_3^{2-}$ solution.

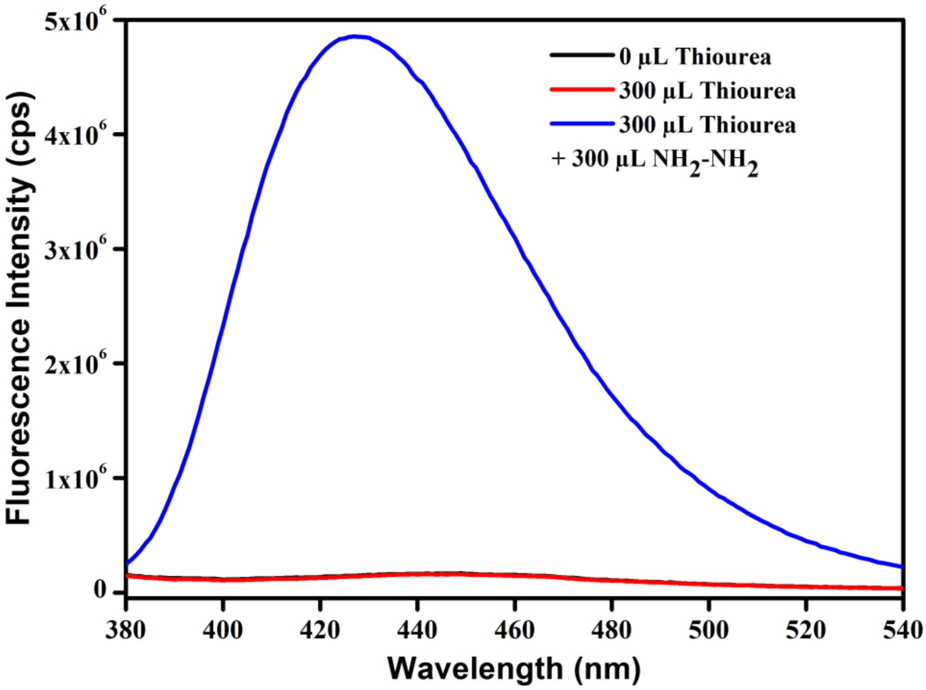

Figure S44. Change in fluorescence emission intensity of probe **Hf-UiO-66-NHCSNHCH$_3$** with the addition of 300 µL of 10 mM aqueous hydrazine solution in the presence of 300 µL of 10 mM aqueous thiourea solution.

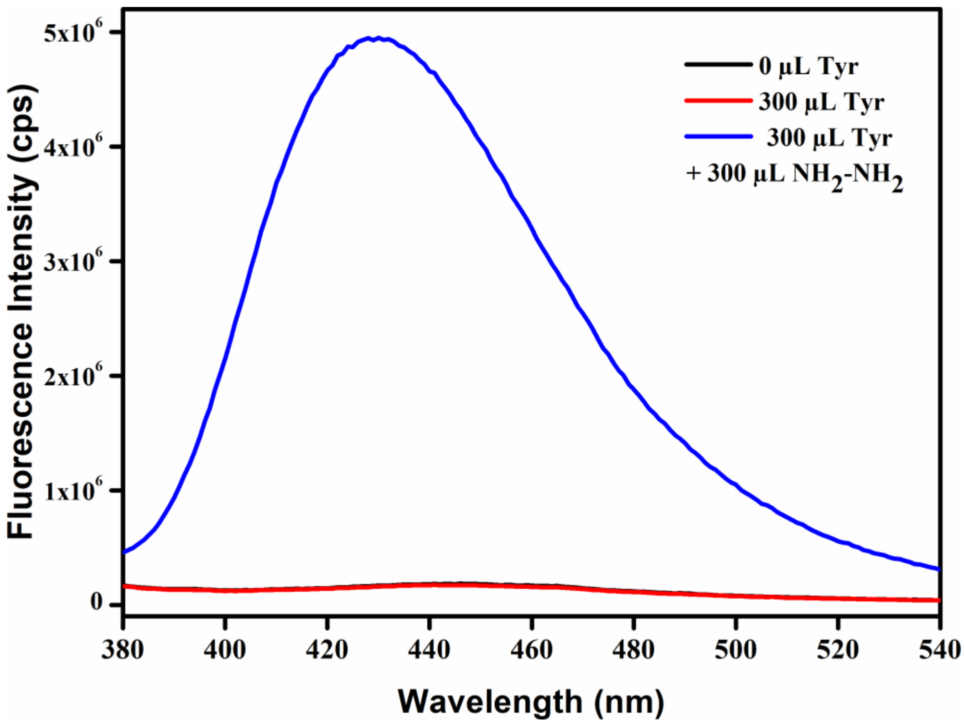

Figure S45. Change in fluorescence emission intensity of probe **Hf-UiO-66-NHCSNHCH$_3$** with the addition of 300 µL of 10 mM aqueous hydrazine solution in the presence of 300 µL of 10 mM aqueous tyrosine solution.

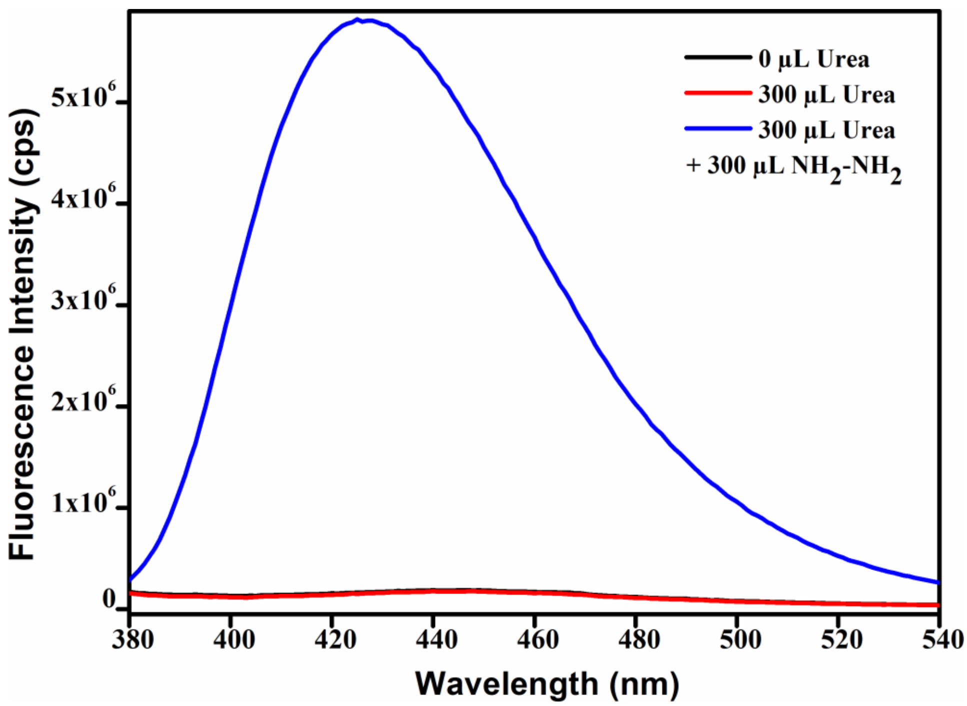

Figure S46. Change in fluorescence emission intensity of probe **Hf-UiO-66-NHCSNHCH$_3$** with the addition of 300 µL of 10 mM aqueous hydrazine solution in the presence of 300 µL of 10 mM aqueous urea solution.

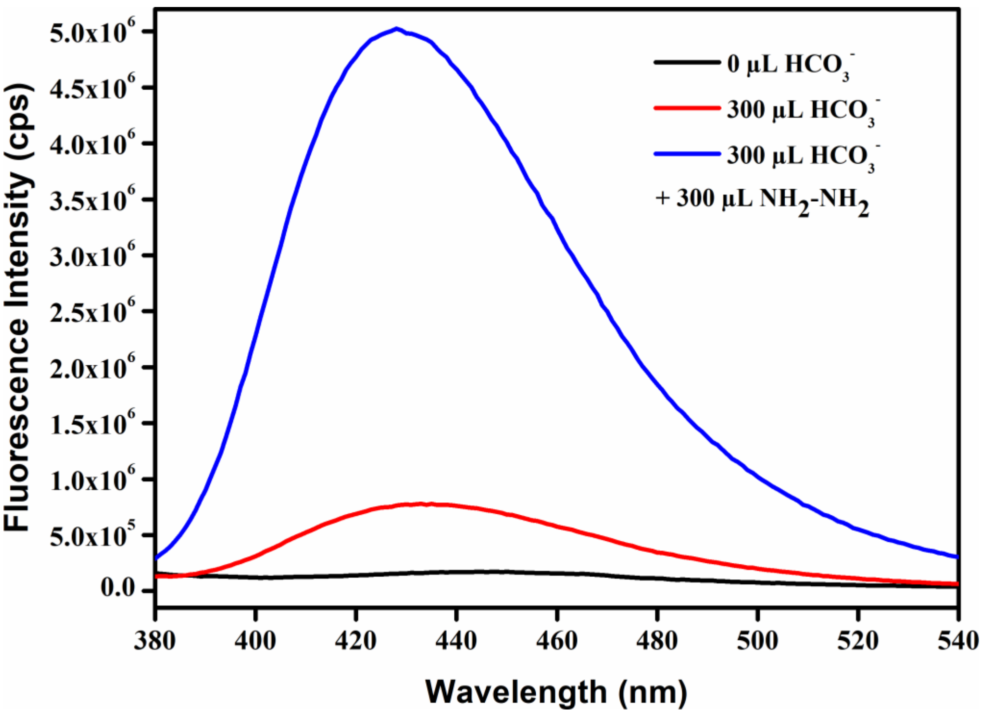

Figure S47. Change in fluorescence emission intensity of probe **Hf-UiO-66-NHCSNHCH$_3$** with the addition of 300 µL of 10 mM aqueous hydrazine solution in the presence of 300 µL of 10 mM aqueous HCO_3^- solution.

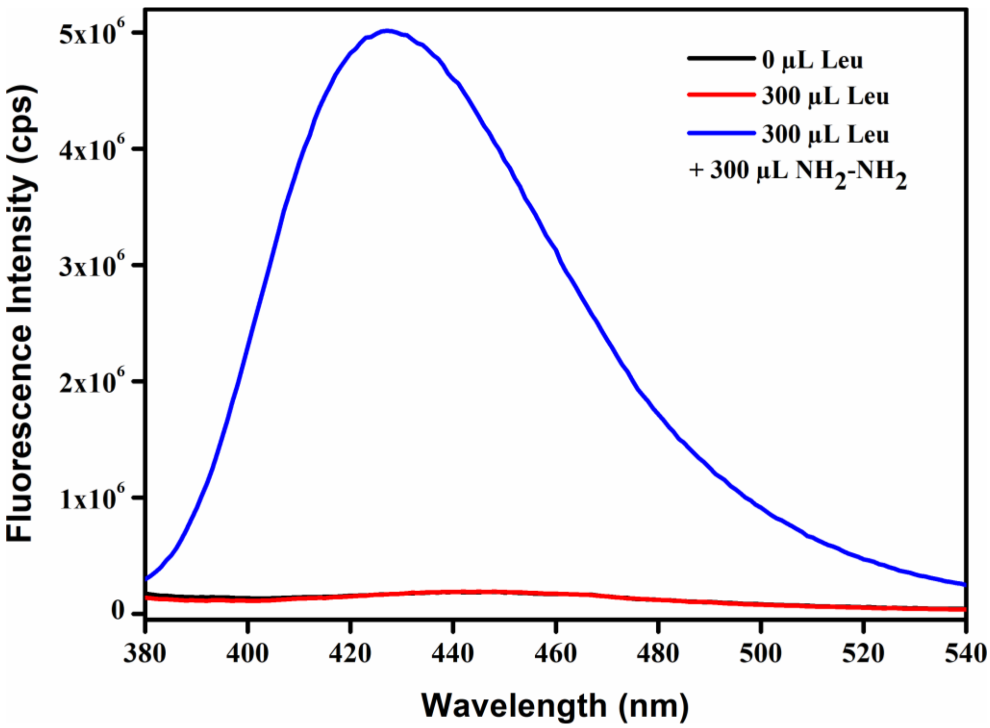

Figure S48. Change in fluorescence emission intensity of probe **Hf-UiO-66-NHCSNHCH$_3$** with the addition of 300 µL of 10 mM aqueous hydrazine solution in the presence of 300 µL of 10 mM aqueous leucine solution.

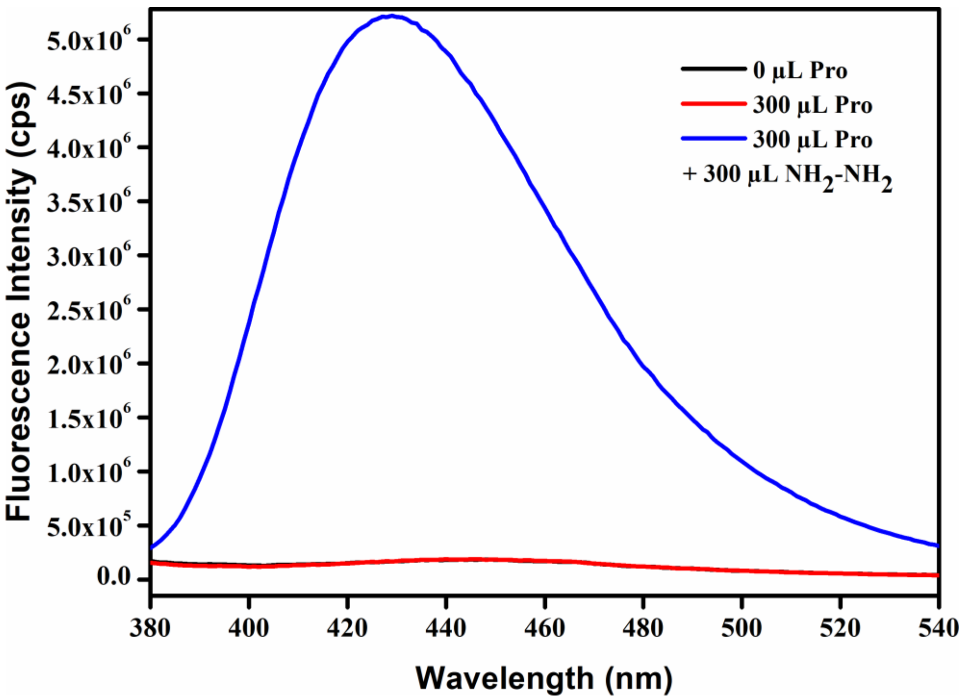

Figure S49. Change in fluorescence emission intensity of probe **Hf-UiO-66-NHCSNHCH$_3$** with the addition of 300 µL of 10 mM aqueous hydrazine solution in the presence of 300 µL of 10 mM aqueous proline solution.

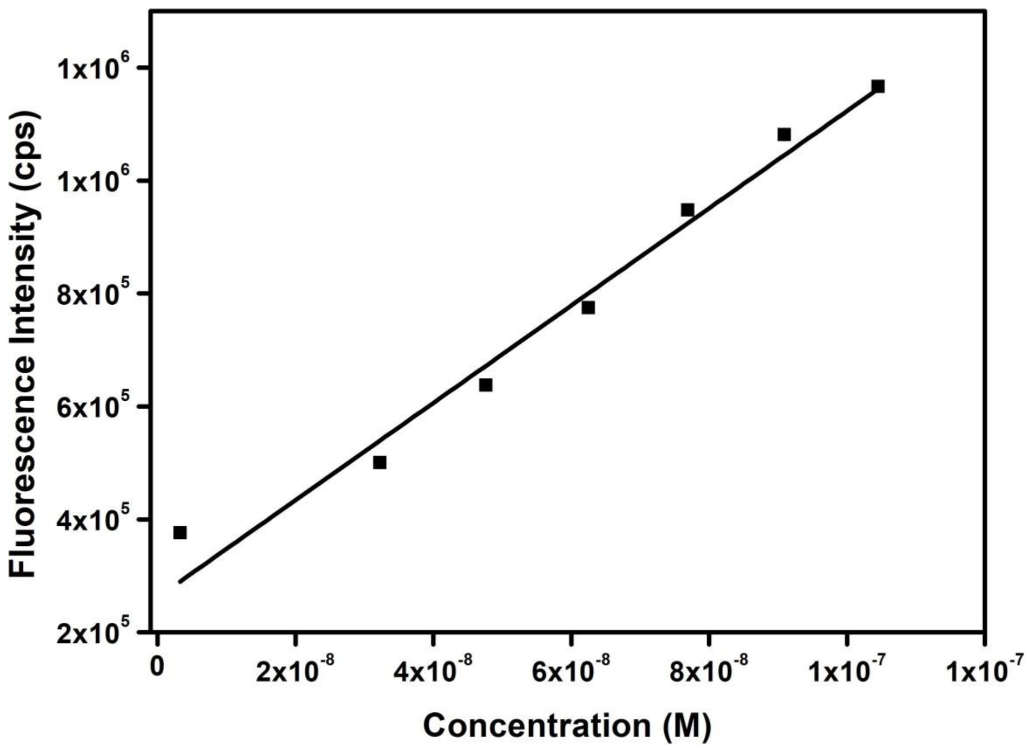

Figure S50. Change in the fluorescence intensity of **Hf-UiO-66-NHCSNHCH$_3$** in water as a function of concentration of NH_2-NH_2 (with error bars).

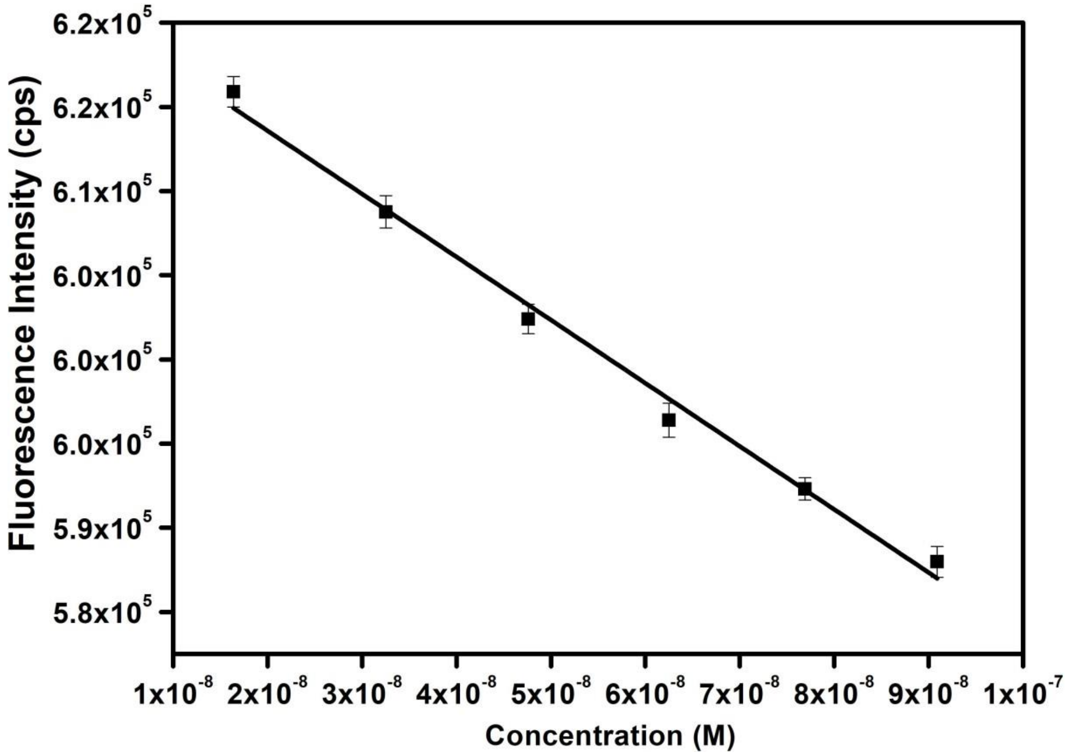

Figure S51. Change in the fluorescence intensity of **Hf-UiO-66-NHCSNHCH$_3$** as a function of concentration of Hg^{2+} (with error bars).

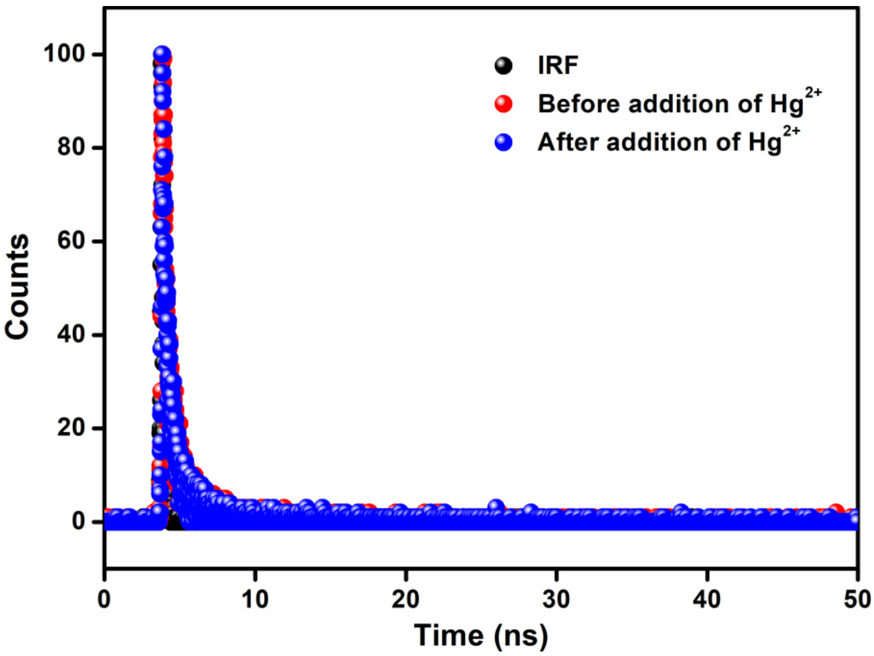

Figure S52. Fluorescence life-time decay curve of probe **Hf-UiO-66-NHCSNHCH$_3$** before and after the addition of Hg^{2+}.

Table S4. Fluorescence life time change (in ns) of probe **Hf-UiO-66-NHCSNHCH$_3$** before and after the addition of 300 µL of aqueous Hg^{2+} solution.

Volume of Hg^{2+} solution added (µL)	B_1	a_1	τ_1 (ns)	$\langle\tau\rangle$* (ns)	χ^2
0	0.0782	1	0.476	0.476	1.054
300	0.0741	1	0.479	0.479	1.001

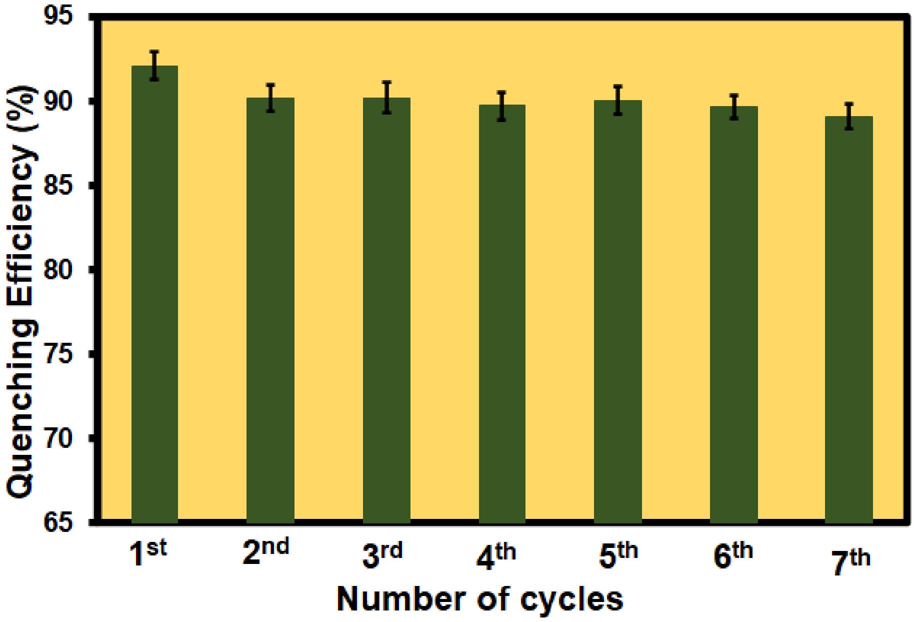

Figure S53. Recyclability of probe **Hf-UiO-66-NHCSNHCH$_3$** towards the detection of Hg^{2+} for 7 cycles with almost equal quenching efficiency up to 7th cycle.

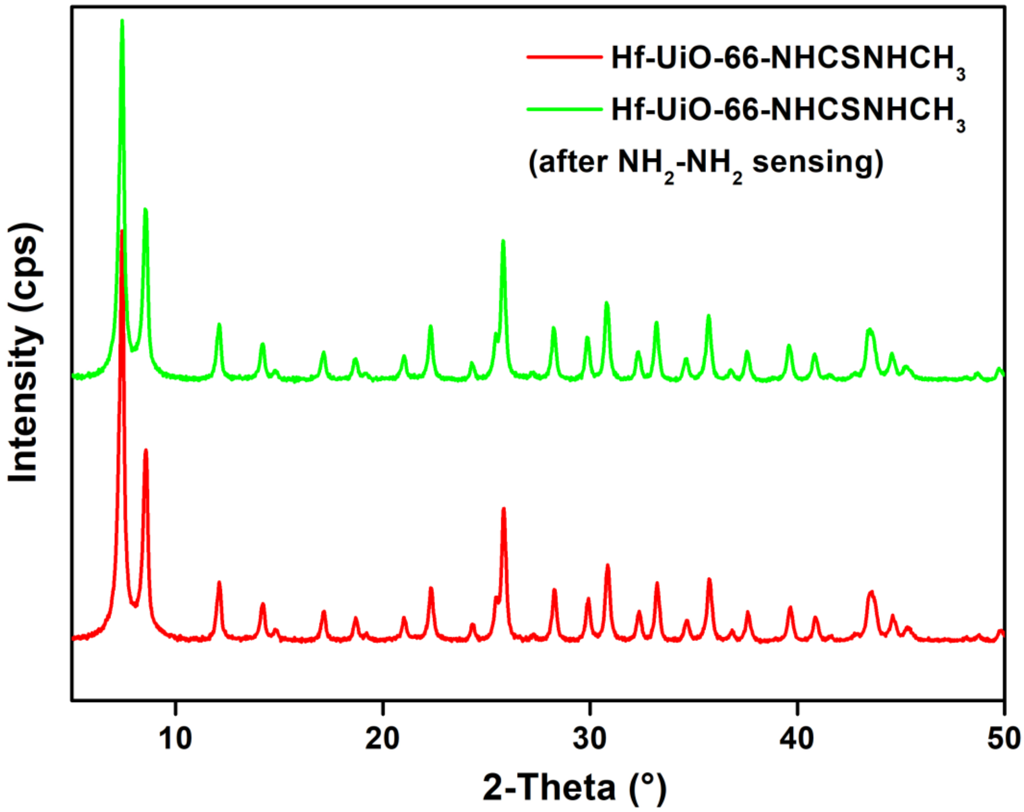

Figure S54. PXRD patterns of **Hf-UiO-66-NHCSNHCH$_3$** before (red) and after (green) sensing of hydrazine.

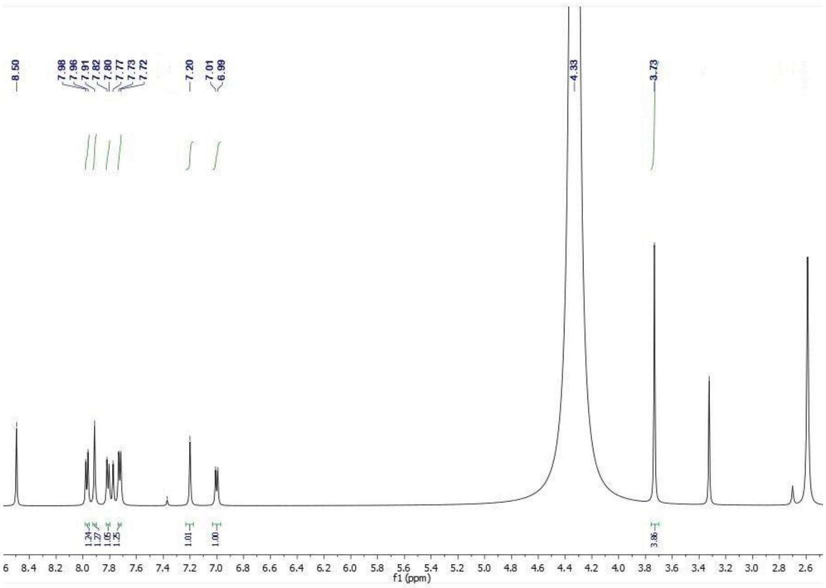

Figure S55. Digested ^{1}H NMR spectrum of **Hf-UiO-66-NHCSNHCH$_3$** after treatment with hydrazine.

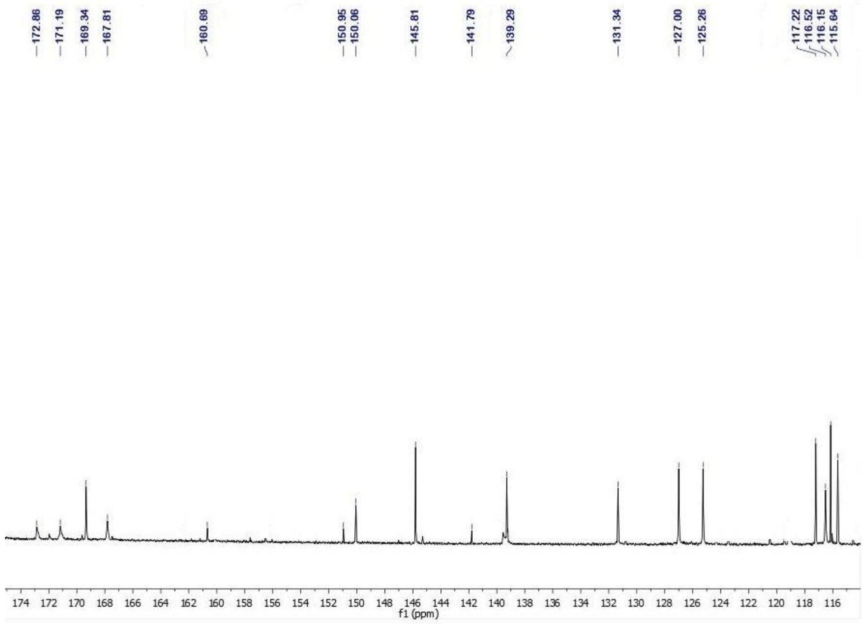

Figure S56. Digested ^{13}C NMR spectrum of **Hf-UiO-66-NHCSNHCH$_3$** after treatment with hydrazine.

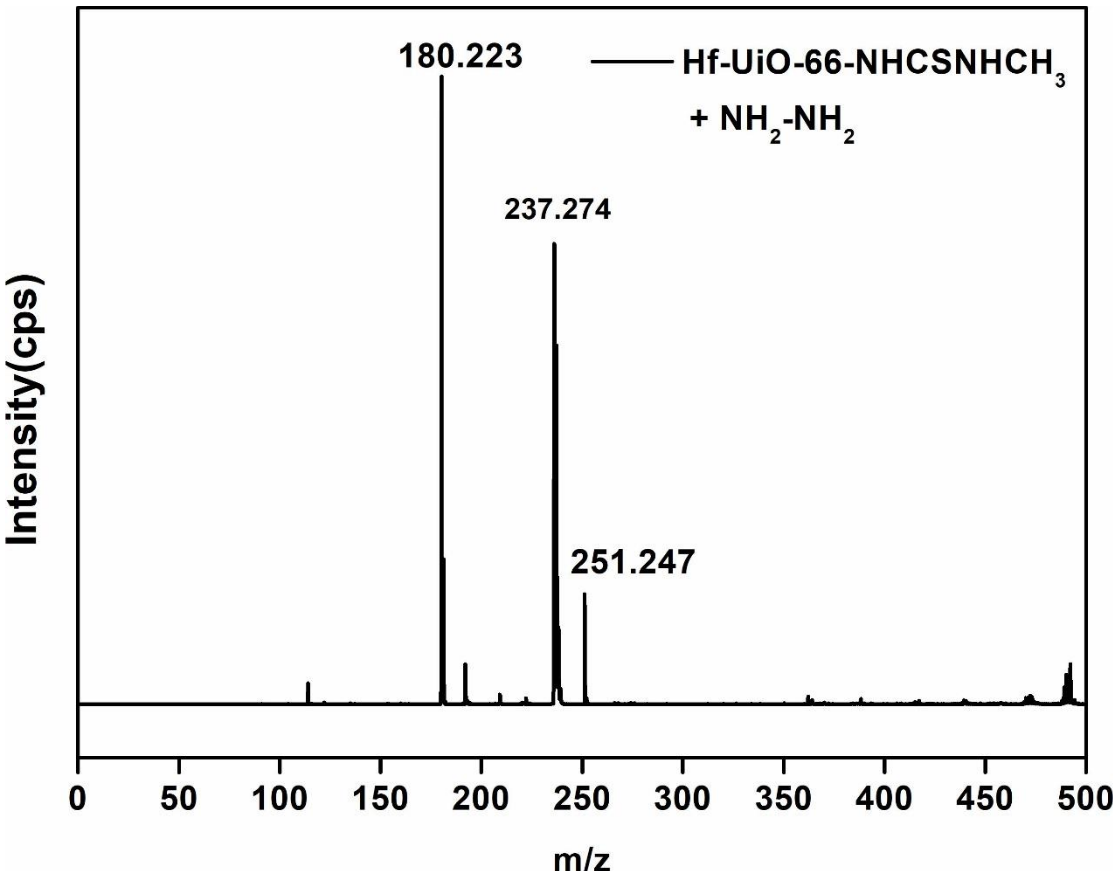

Figure S57. Digested mass spectra spectrum of **Hf-UiO-66-NHCSNHCH$_3$** after treatment with hydrazine in methanol and water mixture.

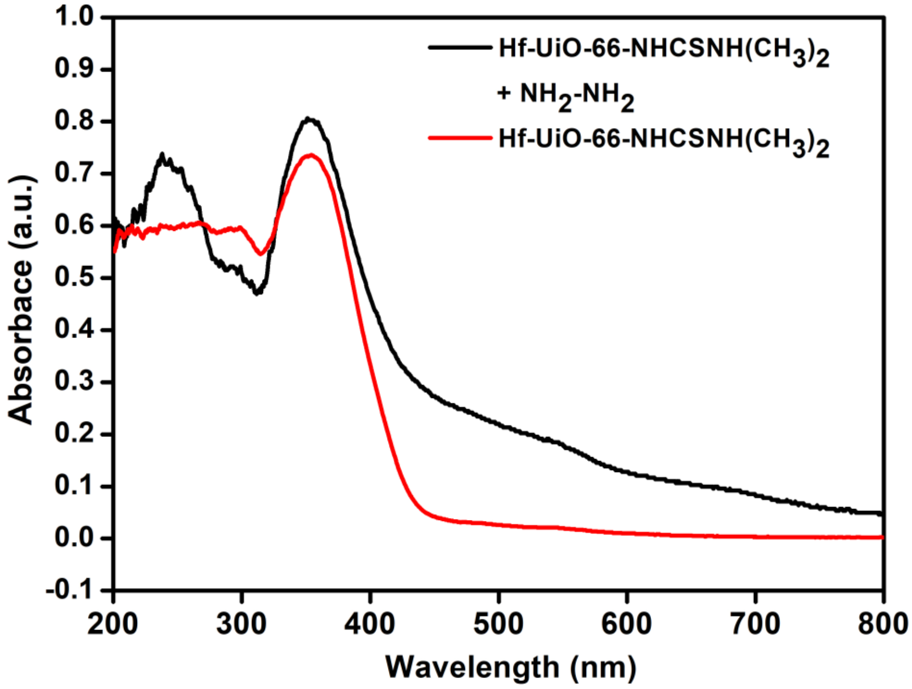

Figure S58. UV-Vis spectrum of **Hf-UiO-66-NHCSNHCH$_3$** before (black) and after (red) sensing of NH_2-NH_2 in solid state.

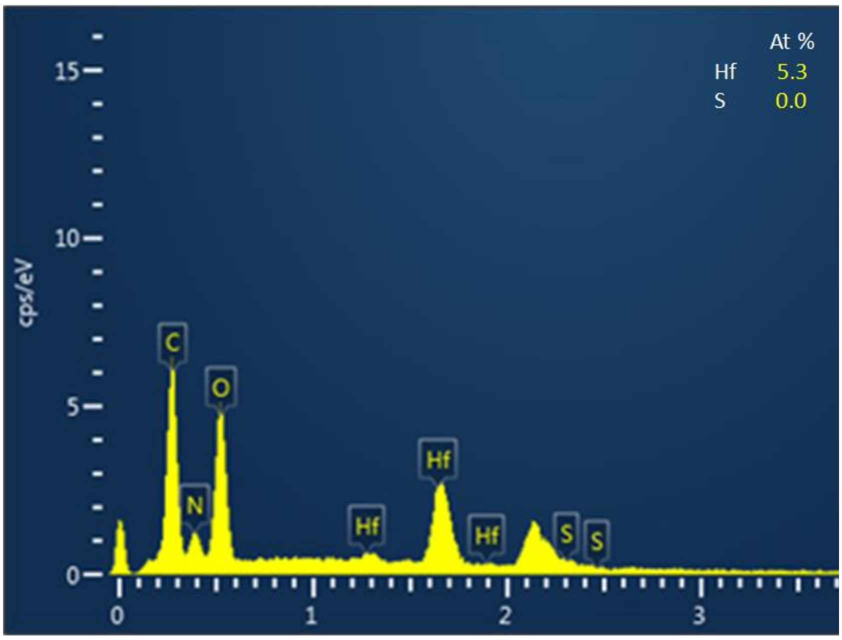

Figure S59. EDX spectrum of recovered **Hf-UiO-66-NHCSNHCH$_3$** after sensing of NH_2-NH_2.

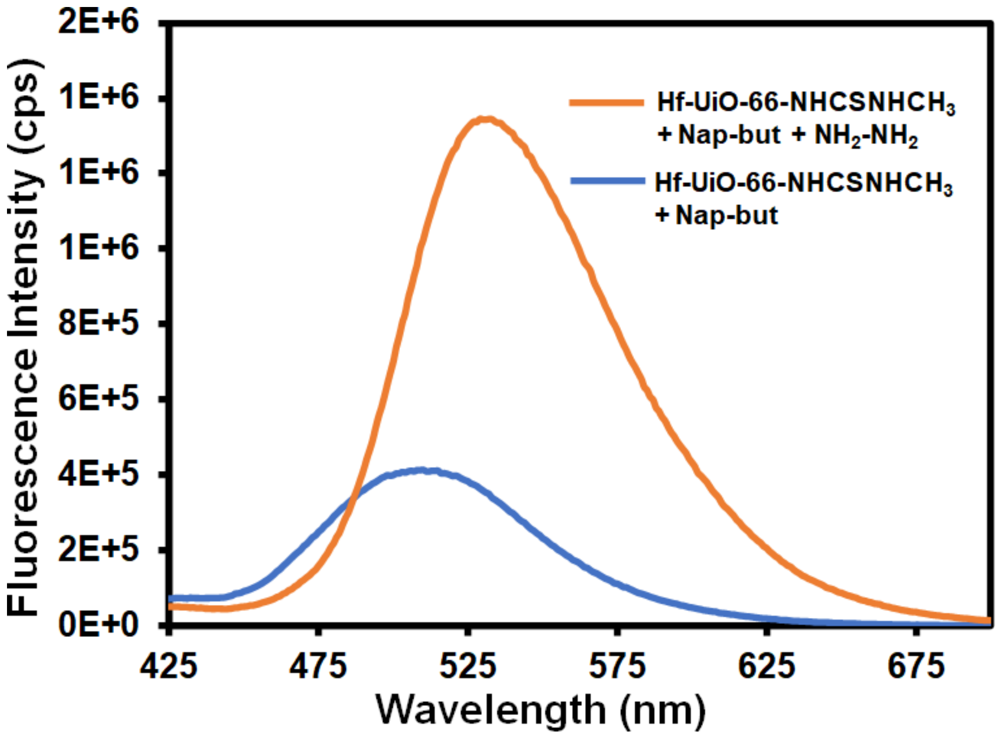

Figure S60. Change in fluorescence emission intensity of **Nap-but** (H_2S sensor) in the presence of probe **Hf-UiO-66-NHCSNHCH$_3$** and after addition of NH_2-NH_2.

Figure S61. Change in colour of **Hf-UiO-66-NHCSNHCH$_3$** + $Pb(CH_3COO)_2$ aqueous mixture after the addition of NH_2-NH_2.

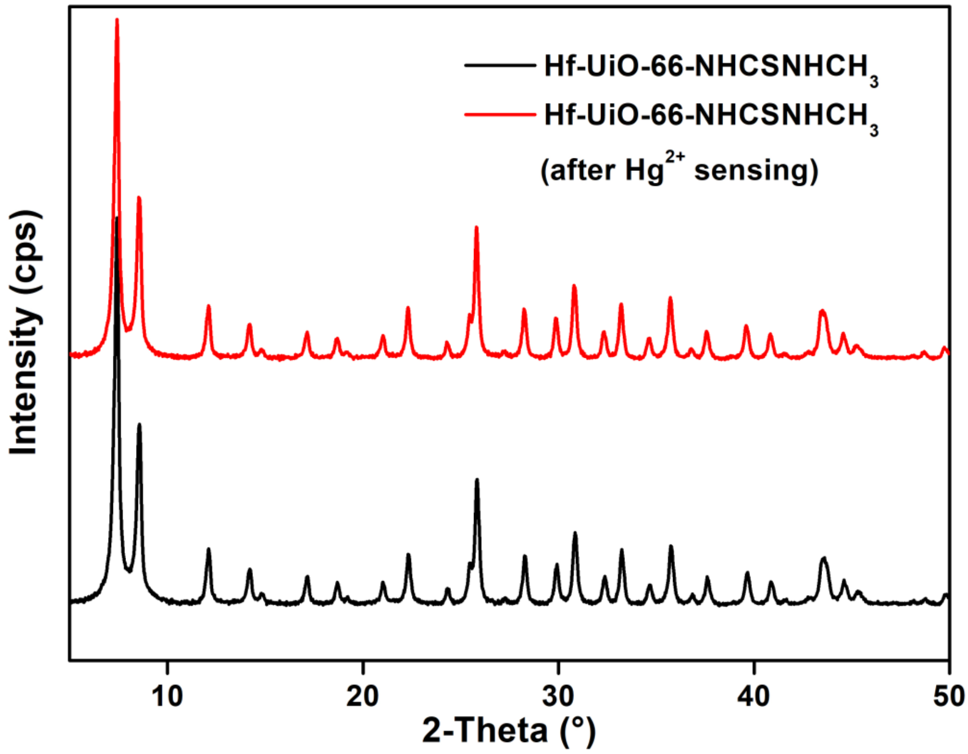

Figure S62. PXRD pattern of **Hf-UiO-66-NHCSNHCH$_3$** before (black) and after (red) the addition of aqueous solution of Hg^{2+}.

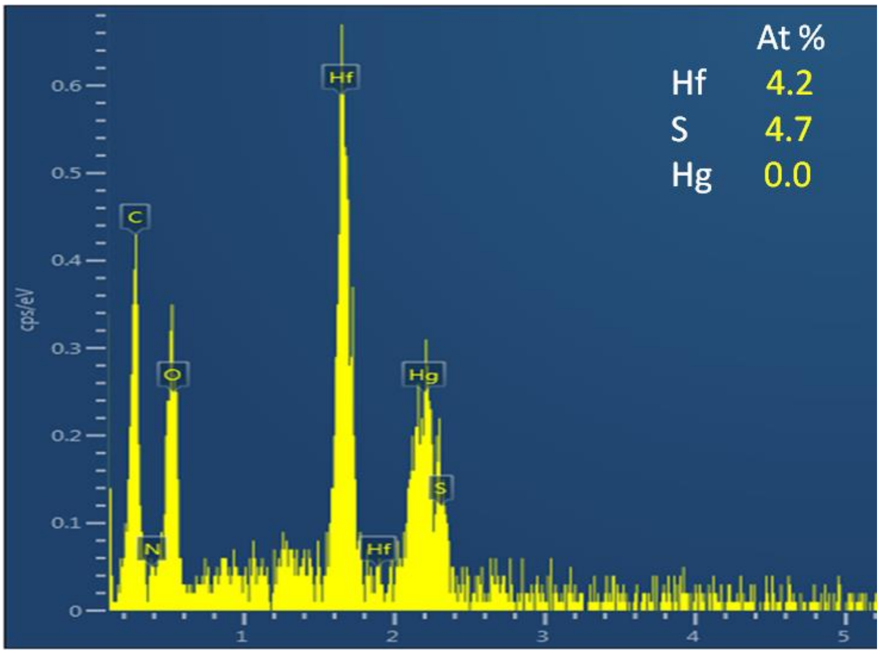

Figure S63. TEM-EDX spectrum of **Hf-UiO-66-NHCSNHCH$_3$** after Hg^{2+} sensing after through washing.

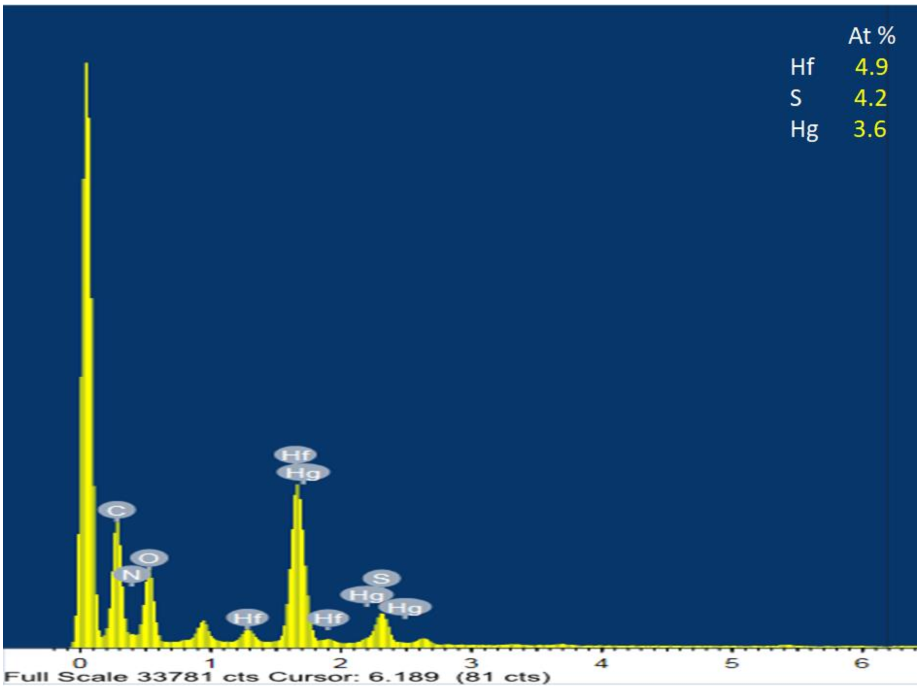

Figure S64. TEM-EDX spectrum of **Hf-UiO-66-NHCSNHCH$_3$** after Hg^{2+} sensing and without through washing.

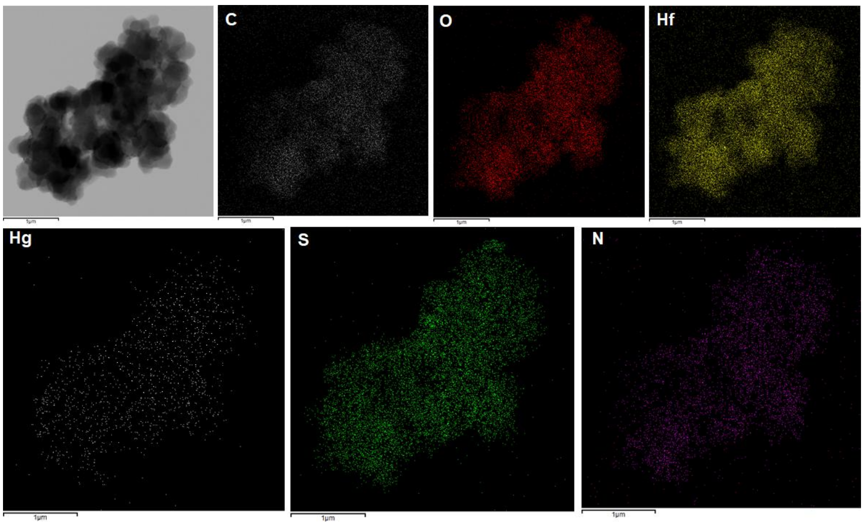

Figure S65. TEM-EDX mapping of **Hf-UiO-66-NHCSNHCH$_3$** after Hg^{2+} sensing and without washing.

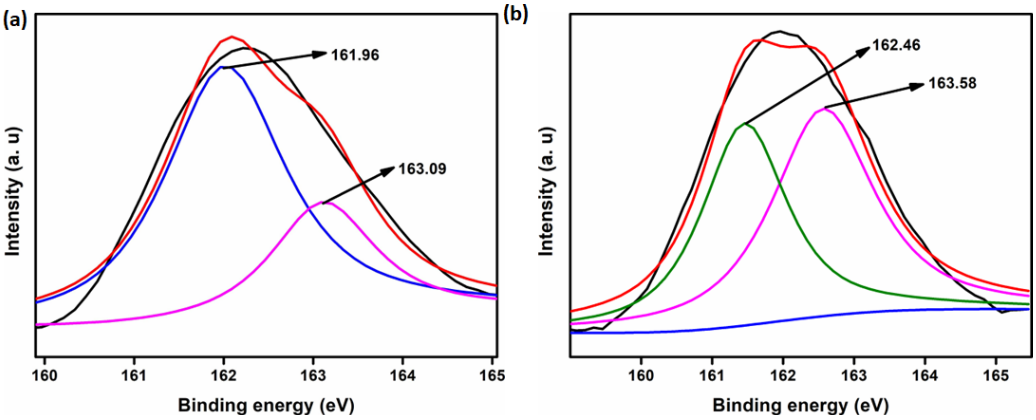

Figure S66. Fitted XPS spectra of S (2s) before (a) and after (b) treatment of Hg^{2+} with **Hf-UiO-66-NHCSNHCH$_3$**.

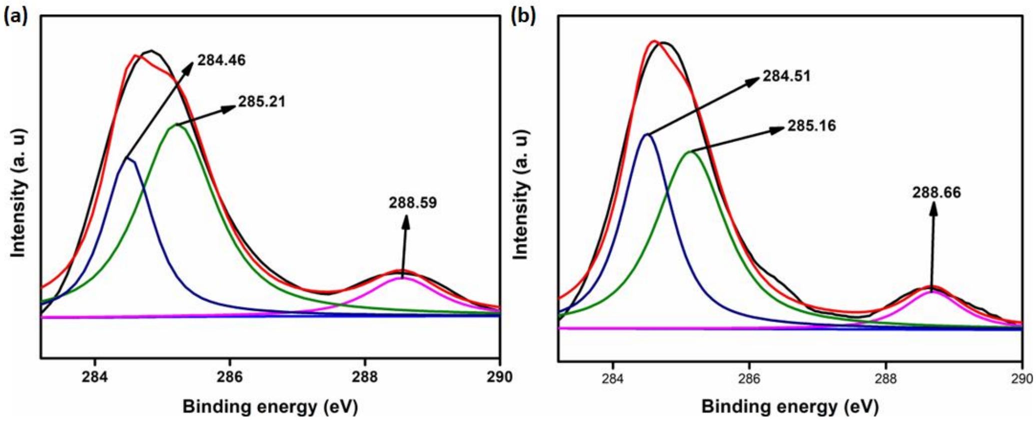

Figure S67. Fitted XPS spectra of C (1s) before (a) and after (b) treatment of Hg^{2+} with **Hf-UiO-66-NHCSNHCH$_3$**.

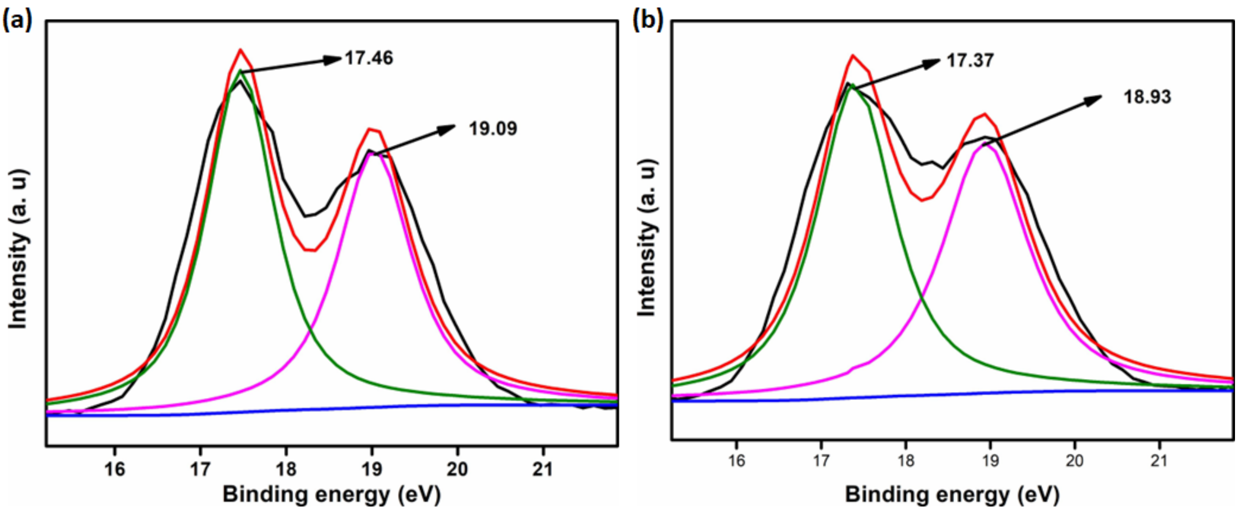

Figure S68. Fitted XPS spectra of Hf (4f) before (a) and after (b) treatment of Hg^{2+} with **Hf-UiO-66-NHCSNHCH$_3$**.

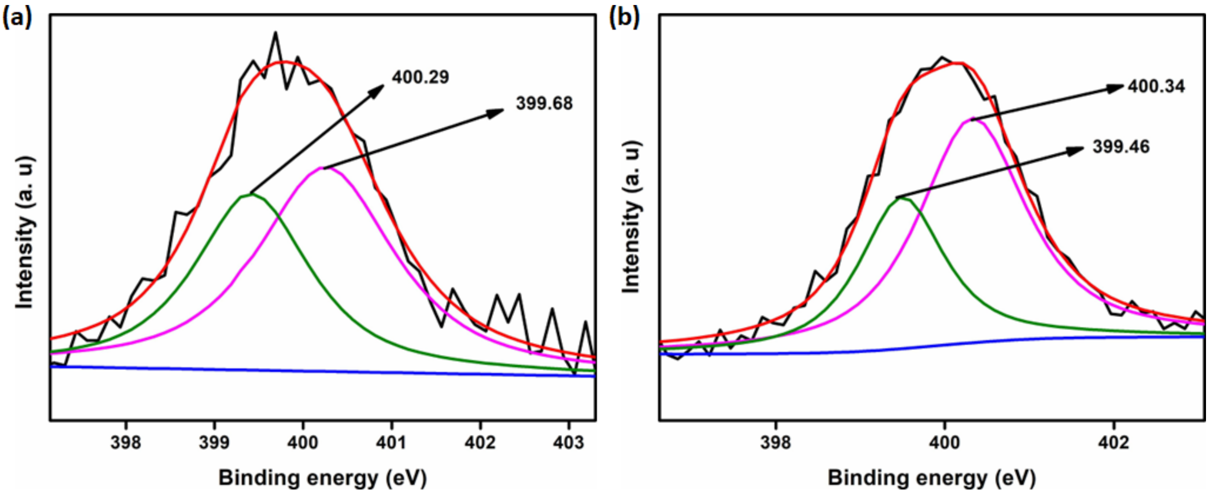

Figure S69. Fitted XPS spectra of N (1s) before (a) and after (b) treatment of Hg^{2+} with **Hf-UiO-66-NHCSNHCH$_3$**.

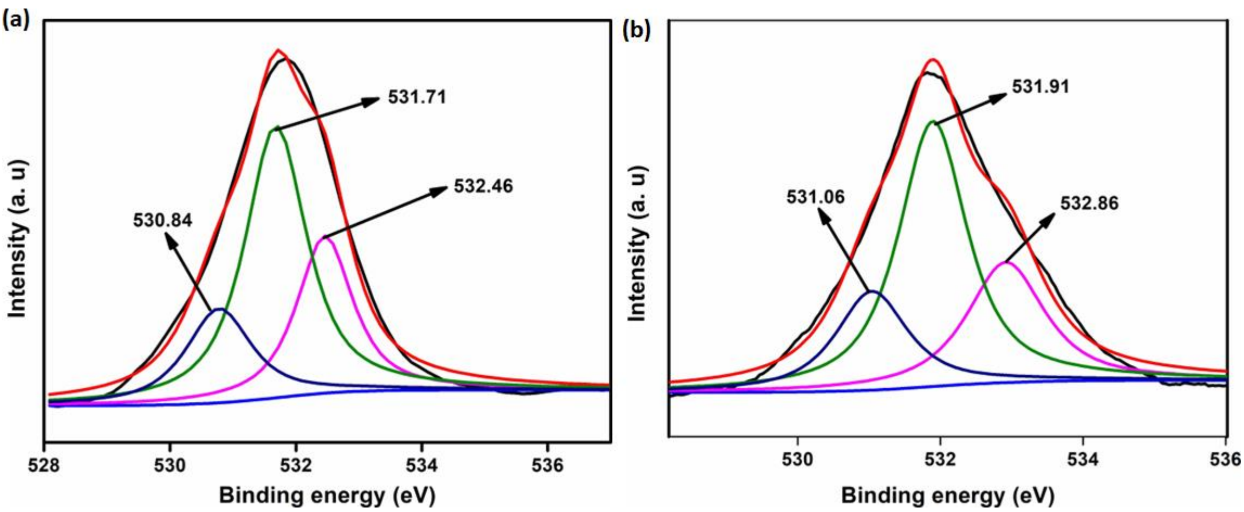

Figure S70. Fitted XPS spectra of O (1s) before (a) and after (b) treatment of Hg^{2+} with **Hf-UiO-66-NHCSNHCH$_3$**.

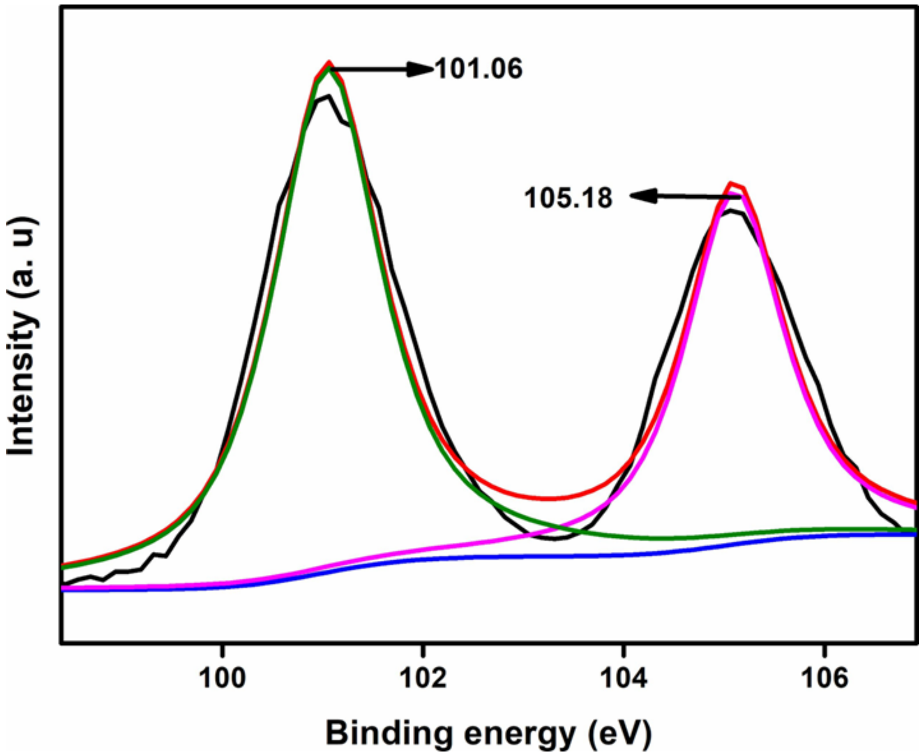

Figure S71. Fitted XPS spectra of Hg (4f) after treatment of Hg^{2+} with **Hf-UiO-66-NHCSNHCH$_3$**.

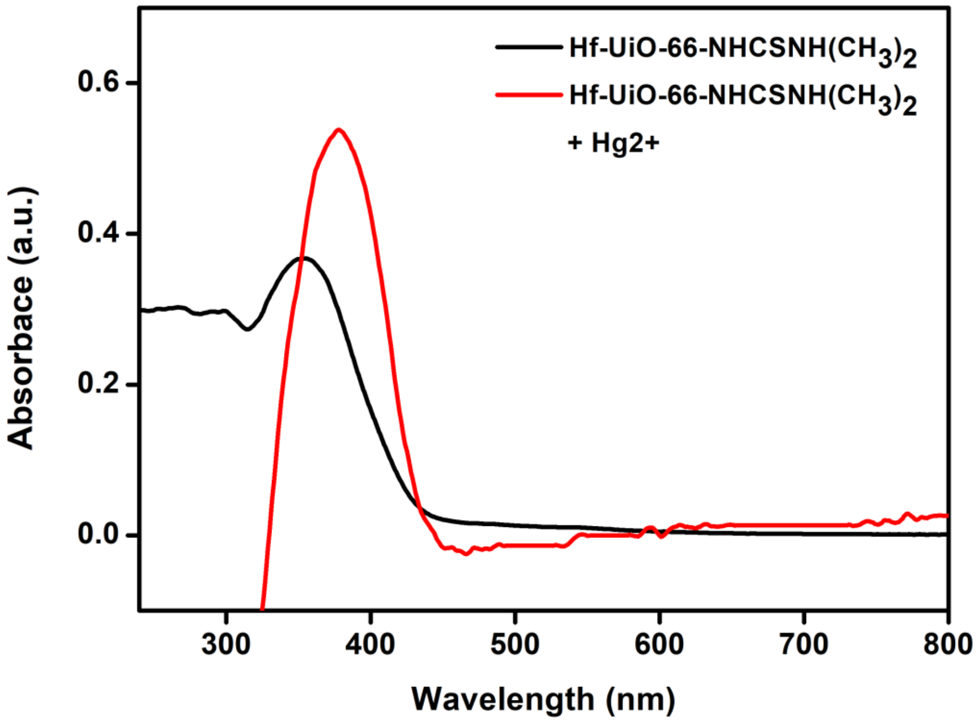

Figure S72. Solid-state UV-Vis spectrum of **Hf-UiO-66-NHCSNHCH$_3$** before (black) and after (red) sensing of Hg^{2+}.

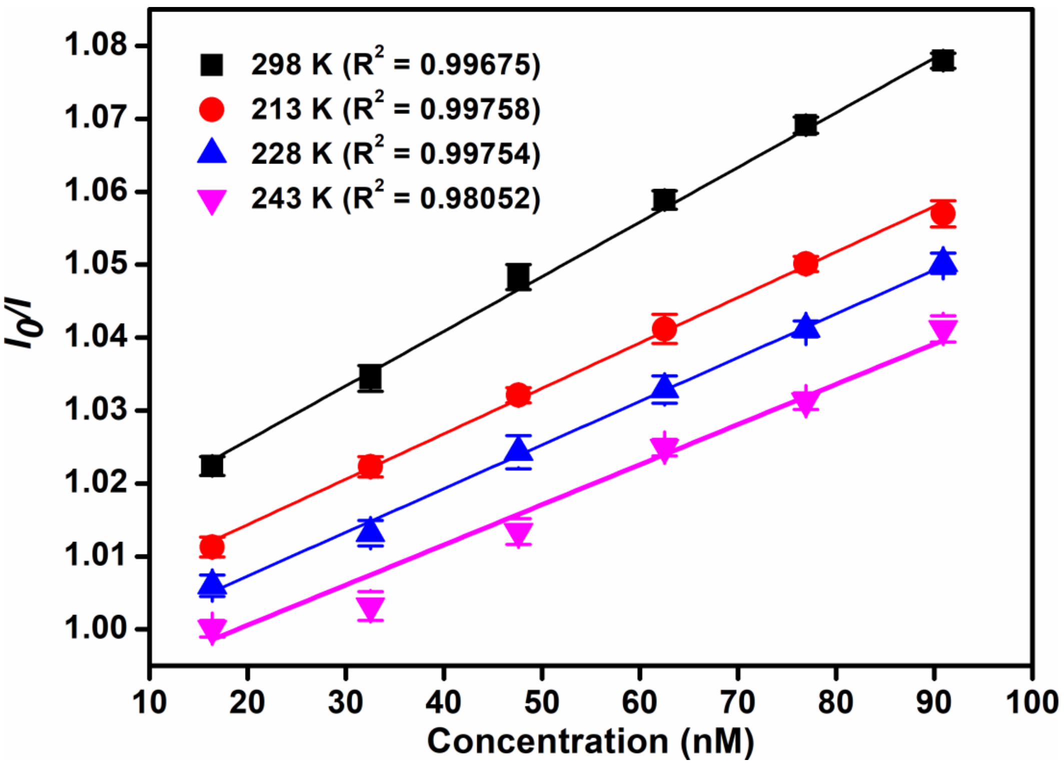

Figure S73. Stern-Volmer plots (with error bars) for fluorescence quenching of **Hf-UiO-66-NHCSNHCH$_3$** by Hg^{2+} at different temperatures.

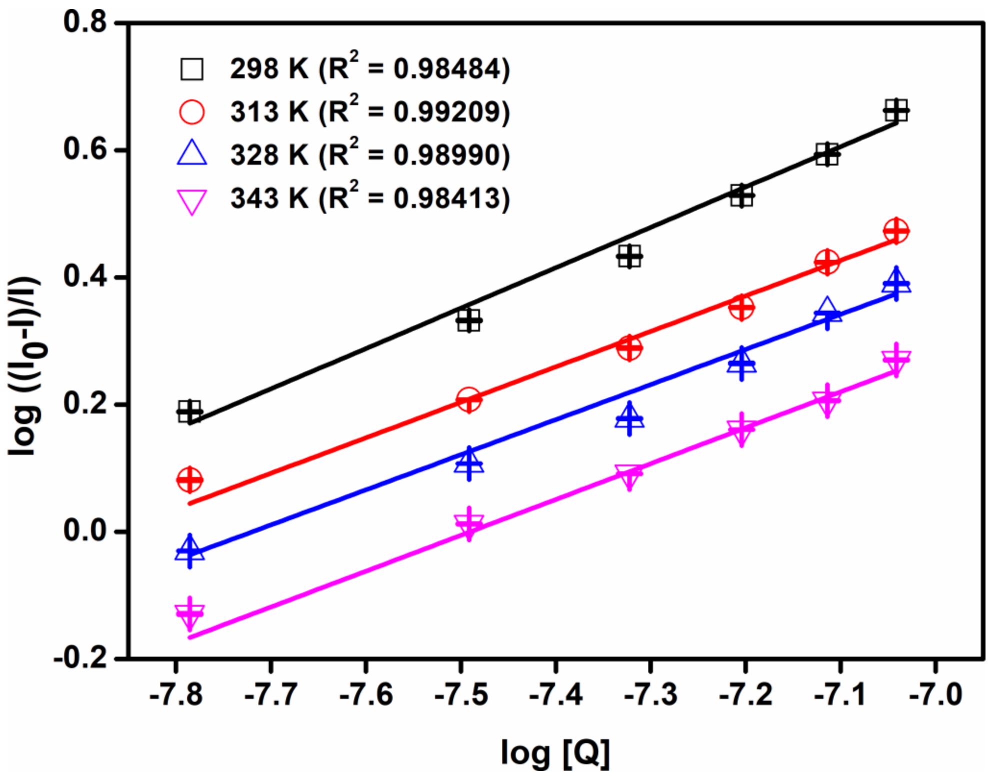

Figure S74. Modified Stern-Volmer plots (with error bars) between log((I_0-I)/I) and log [Q].

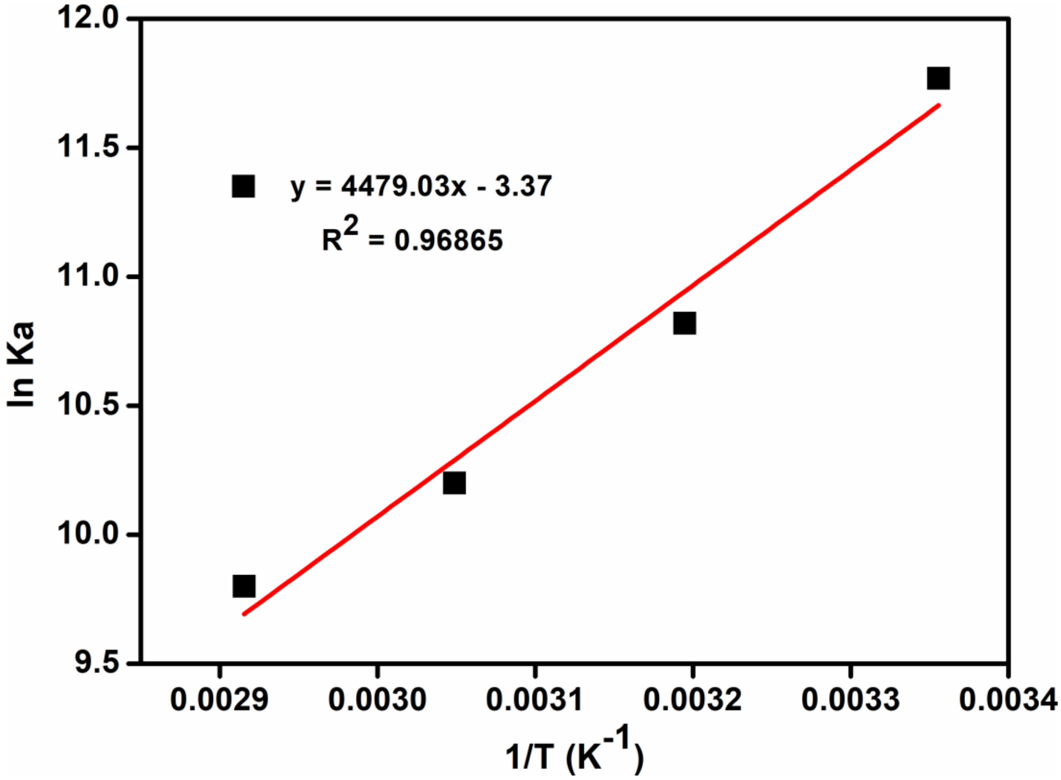

Figure S75. Van't Hoff plot for interaction of **Hf-UiO-66-NHCSNHCH$_3$** with Hg^{2+}.

Table S5. Comparison of the response time, detection limit and sensing media used for the reported fluorescent chemosensors of NH_2-NH_2 in the literature.

Sl. No.	Sensor Material	Type of Material	Sensing Medium	Mode of Detection	Detection Limit	Response Time	Ref.
1	$[Zr_6O_4(OH)_4(BDC\text{-}O\text{-}SO_2\text{-}Ph\text{-}NO_2)_6]\cdot 11H_2O\cdot 4DMF$	MOF	water	turn-on	52.6 nM	2 min	2
2	Zr-UiO-66-$(OCOCH_3)_2$	MOF	water	turn-on	78.8 nM	seconds	3
3	UiO-66-phmd	MOF	HEPES buffer	turn-on	0.87 µM	20 min	4
4	BTI	organic-molecule	HEPES buffer	turn-on	2.9 ppb	20 min	5
5	HyP-1	organic-molecule	PBS buffer	turn-on	0.035 ppb	1 h	6
6	P1	organic-molecule	PRS buffer	turn-on	1.79 nM	40 s	7
7	BPB	BODIPY-based organic molecule	HEPES buffer	turn-off	1.87 µM	-	8

8	Naphsulf-O	Organic-molecule	PBS buffer	turn-on	22 nM	40 min	9
9	BBHC	Organic-molecule	PBS buffer	turn-on	0.43 µM	1 min	10
10	CFAc	Organic-molecule	PBS buffer	ratio-metric	0.0474 µM	-	11
11	BI-E	near-infrared fluorescent probe	PBS buffer	turn-on	0.057 µM	1 min	12
12	NA-N_2H_4	naphthalimide based organic molecule	HEPES buffer	ratio-metric	9.4 nM	15 min	13
13	TAPHP	organic-molecule	HEPES buffer	ratio-metric	0.3 µM	60 min	14
14	AB-NDI	organic-molecule	DMSO	turn-on	-	-	15
15	TNQ	organic-molecule	PBS buffer	ratio-metric	-	-	16
16	HBTM	organic-molecule	PBS buffer	turn-on	29 µM	55 min	17
17	NAC	naphthalene based organic molecule	HEPES buffer	turn-on	4.5 µM	4 min	18
18	DPA	organic-molecule	DMSO/ PBS buffer solution (4/6, v/v)	turn-on	1.9 nM	8 min	19
19	probe **1** probe **2**	pyrene- and anthracenebased organic molecule	HEPES buffer	turn-on	0.17 µM 0.24 µM	3 min	20
20	SF-Azo compounds	organic-molecule	CH_3OH/H_2O (v/v = 1:1)	turn-on	2.33 mM	18-42 min	21
21	levulinated hydroxyl-coumarin 1	organic-molecule	acetate buffer	turn-on	2.46 µM	15 min	22
22	Compound **6a**	organic-molecule	HEPES/ DMSO (1:1, v/v)	turn-on and ratiometric	0.19 µM	-	23
23	NS-N_2H_4	organic-molecule	PBS/ DMSO (v/v = 2/1)	turn-on	-	240 min	24
24	PBF	organic-molecule	CH_3CN–H_2O (6: 4, v/v)	turn-on	0.41 µM	1 min	25
25	Hf-UiO-66-$NHCSNHCH_3$	MOF	H_2O	turn-on	1.9 nM	0.8 min	this work

Table S6. Comparison of the response time, detection limit and sensing media used for the reported chemosensors of Hg^{2+} in the literature using fluorometric method.

Sl. No.	Sensor Material	Type of Material	Sensing Medium	Detection Limit (nM)	Response Time (min)	Ref.
1	Thiosemicarbazone	organic-molecule	0.01 M acetic acid/sodium acetate buffer	770	-	26
2	GT capped AgNPs	nanoparticles	water	0.037	0-60	27
3	Azo Crown ether	organic molecule	methanol	13900	-	28
4	Rhodamine 6 G based	Rh-complex	THF: Water (8:2, v/v, pH = 7)	30.37	-	29
5	Tetraphenyl ethylene based AIE probe	organic molecule	water	63	-	30
6	Squaraine based fluorescent probe	organic molecule	Ethanol: Water (20:80, v/v)	21.9	3	31
7	Rhodamine appended terphenyl	organic molecule	THF	500	30	32
8	Double naphthalene Schiff base	organic compound	DMSO	55.9	80	33
9	2-Hydroxy benzothiazole modified rhodol	organic compound	THF: HEPES (4:6, v/v)	270	-	34
10	Nitrogen-doped carbon quantum dots	quantum dots	water	230	15	35
11	$[Ni(3\text{-}bpd)_2(NCS)_2]_n$	MOF	water	-	120	36
12	[PCN-221]	MOF	water	10	1	37
13	[Cu(Dcbb)(Bpe)].Cl	MOF	HEPES buffer	3.2 and 3.3	30	38
14	UiO-66@ Butyne	MOF	water	10.9	3	39

15	Ln(TATAB) .(DMF)$_4$ (H$_2$O)(MeOH)$_{0.5}$	MOF	water	4.4	-	40
16	Eu^{3+}/CDs@MOF-253	MOF	water	47.88	3	41
17	[Cu(Cdcbp)(H$_2$O)2·2H 2O]$_n$	MOF	water	2.3	2	42
18	Al-MOF (TAM)	MOF	water	2.94	0.5	43
19	[Cu(Cbdcp)(Dps) (H$_2$O)$_3$]·6H$_2$O$_n$	MOF	HEPES buffer	2.6	10	44
20	Cd−EDDA	MOF	water	2	0.25	45
21	tetrahydrodibenzo phenanthridine derivatives	organic compound	DMSO : THF = 1 : 1	0.91 0.041	1	46
22	[Zn(L)(BBI).(H$_2$O)$_2$] [Cd(L)(TPOM)0$_{.75}$]·xS	MOF	water	-		47
33	IITG-5a	MOF	water	5	1	48
34	Hf-UiO-66-NHCSNHCH$_3$	MOF	H_2O	4	0.16	this work

References:

(1) Jakobsen, S.; Gianolio, D.; Wragg, D. S.; Nilsen, M. H.; Emerich, H.; Bordiga, S.; Lamberti, C.; Olsbye, U.; Tilset, M.; Lillerud, K. P. Structural determination of a highly stable metal-organic framework with possible application to interim radioactive waste scavenging: Hf-UiO-66. *Phys. Rev. B* **2012**, *86*, 125429.
(2) Ghosh, S.; Biswas, S. A functionalized UiO-66 metal-organic framework acting as a fluorescent based selective sensor of hydrazine in aqueous medium. *Microporous Mesoporous Mater.* **2022**, *329*, 111552.
(3) Nandi, S.; SK, M.; Biswas, S. Rapid Switch-On Fluorescent Detection of Nanomolar Level Hydrazine in Water by a Diacetoxy Functionalized MOF: Application in Paper Strips and Environmental Samples. *Dalton Trans.* **2020**, *49*, 2830-2834.
(4) SK, M.; Khan, M. R. U. Z.; Das, A.; Nandi, S.; TrivedI, V.; Biswas, S. A Phthalimide-functionalized UiO-66 Metal–organic Framework for the Fluorogenic Detection of Hydrazine in Live Cells. *Dalton Trans.* **2019**, *48*, 12615-12621.
(5) Maji, R.; Mahapatra, A. K.; Maiti, K.; Mondal, S.; Ali, S. S.; Sahoo, P.; Mandal, S.; Uddin, M. R.; Goswami, S.; Quah, C. K.; et al. A Highly Sensitive Fluorescent Probe for Detection of Hydrazine in Gas and Solution Phases Based on the Gabriel mechanism and its Bioimaging. *RSC Adv.* **2016**, *6*, 70855-70862.

(6) Jung, Y.; Ju, I. G.; Choe, Y. H.; Kim, Y.; Park, S.; Hyun, Y.-M.; Oh, M. S.; D. Kim. Hydrazine Expose: The Next-Generation Fluorescent Probe. *ACS Sens.* **2019**, *4*, 441-449.
(7) Shweta, S.; Kumar, A.; Asthana, S. K.; Prakash, A.; Roy, J. K.; Tiwari, I.; Upadhyay, K. K. A two-step Continuous Synthesis of α-ketoamides and α-amino Ketones from 2° Benzylic Alcohols Using Hydrogen Peroxide as an Economic and Benign Oxidan. *RSC Adv.* **2016**, *6*, 94959-99496.
(8) Mahapatra, A. K.; Maji, R.; Maiti, K.; Manna, S. K.; Mondal, S.; Ali, S. S.; Manna, S.; Sahoo, P.; Mandal, S.; Uddin, M. R.; et al. A BODIPY/pyrene-based Chemodosimetric Fluorescent Chemosensor for Selective Sensing of Hydrazine in the Gas and Aqueous Solution State and its Imaging in Living Cells. *RSC Adv.* **2015**, *5*, 58228-58236.
(9) Chen, W.; Liu, W.; Liu, X.-J.; Kuang, Y.-Q.; Yu, R.-Q.; J.-H.Jiang. A Novel Fluorescent Probe for Sensitive Detection and Imaging of Hydrazine in Living Cells. *Talanta* **2017**, *162*, 225-231.
(10) Paul, S.; Nandi, R.; Ghoshal, K.; Bhattacharyya, M.; Maiti, D. K. A Smart Sensor for Rapid Detection of Lethal Hydrazine in Human Blood and Drinking Water. *New J. Chem.* **2019**, *43*, 3303-3330.
(11) Zhang, Z.; Zhuang, Z.; Song, L. L.; Lin, X.; Zhang, S.; Zheng, G.; Zhan, F. A FRET-based Ratiometric Fluorescent Probe for Hydrazine and its Application in Living Cells. *J. Photochem. Photobiol. A* **2018**, *358*, 10-16.
(12) Ma, J.; Fan, J.; Li, H.; Yao, Q.; Xia, J.; Wang, J.; Peng, X. Probing Hydrazine with a Near-infrared Fluorescent Chemodosimeter. *Dyes Pigm.* **2017**, *138*, 39-46.
(13) Xia, X.; Zeng, F.; Zhang, P.; Lyu, J.; Huang, Y.; Wu, S. An ICT-based Ratiometric Fluorescent Probe for Hydrazine Detection and its Application in Living Cells and in Vivo. *Sens. Actuators B* **2017**, *227*, 411-418.
(14) Luo, Z.; Liu, B.; Qin, T.; Zhu, K.; Zhao, C.; Pan, C.; Eang, L. Cyclization of Chalcone Enables Ratiometric Fluorescence Determination of Hydrazine with a High Selectivity. *Sens. Actuators B* **2018**, *263*, 229-236.
(15) Zhou, D.; Wang, Y.; Jia, J.; Yu, W.; Qu, B.; Li, X.; Sun, X. H-Bonding and Charging Mediated Aggregation and Emission for Fluorescence Turn-on Detection of Hydrazine Hydrate. *Chem. Commun.* **2015**, *51*, 10656-10659.
(16) Yu, S.; Wang, S.; Yu, H.; Feng, Y.; Zhang, S.; Zhu, M.; Yin, H.; Meng, X. A Ratiometric Two-photon Fluorescent Probe for Hydrazine and its Applications. *Sens. Actuators B* **2015**, *220*, 1338-1345.
(17) Chen, Z.; Zhong, X.; Qu, W.; Shi, T.; Liu, H.; He, H.; Zhang, X.; Wang, S. A Highly Selective HBT-based “Turn-on” Fluorescent Probe for Hydrazine Detection and its Application. *Tetrahedron Lett.* **2017**, *58*, 2596-2601.
(18) Goswami, S.; Das, A. K.; Saha, U.; Maity, S.; Khanra, K.; Bhattacharyya, N. Rapid Detection of Hydrazine in a Naphthol-fused Chromenyl Loop and its Effectiveness in Human Lung Cancer Cells: Tuning Remarkable Selectivity Via the Reaction Altered Pathway Supported by Theoretical Studies. *Org. Biomol. Chem.* **2015**, *13*, 2134-2139.
(19) Zhang, Y.; Huang, Y.; Yue, Y.; Chao, J.; Huo, F.; Yin, C. A Compact Fluorescent Probe Based on o-phthalaldehyde for Ultrasensitive Detection of Hydrazine in Gas and Solution Phases. *Sens. Actuators B* **2018**, *273*, 944-950.
(20) Roy, B.; Halder, S.; Guha, A.; Bandyopadhyay, S. Hydrazine-Selective Fluorescent Turn-On Probe Based on Ortho-Methoxy-Methyl-Ether (o-MOM) Assisted Retro-aza-Henry Type Reaction. *Anal. Chem.* **2017**, *89*, 10625-10636.
(21) Shin, M. C.; Lee, Y.; Park, S. B.; Kim, E. Development of Azo-based Turn-on Chemical Array System for Hydrazine Detection with Fluorescence Pattern Analysis. *ACS Omega* **2019**, *4*, 14875-14885.

(22) Choi, M. G.; Hwang, J.; Moon, J. O.; Sung, J.; Chang, S.-K. Hydrazine-selective Chromogenic and Fluorogenic Probe Based on Levulinated Coumarin. *Org. Lett.* **2011**, *13*, 5260-5263.
(23) Purohit, D.; Sharma, C. P.; Raghuvanshi, A.; Jain, A.; S.Rawat, K.; M.Gupta, N.; Singh, J.; Sachdev, M.; Goel, A. First Dual Responsive "Turn-On" and "Ratiometric" AIEgen Probe for Selective Detection of Hydrazine Both in Solution and the Vapour Phase. *Chem. Eur.J.* **2019**, *25*, 4660-4664.
(24) Wang, J.-Y.; Liu, Z.-R.; Ren, M.; Lin, W. 2-benzothiazoleacetonitrile Based Two-photon Fluorescent Probe for Hydrazine and its Bio-imaging and Environmental Applications. *Sci. Rep.* **2017**, *7*, 1-8.
(25) Goswami, S.; Paul, S.; Manna, A. Fast and Ratiometric ''Naked Eye'' Detection of Hydrazine for Both Solid and Vapour Phase Sensing. *New J. Chem.* **2015**, *39*, 2300-2305.
(26) Yu, Y.; Lin, L.-R.; Yang, K.-B.; Zhong, X.; Huang, R.-B.; Zheng, L.-S. p-Dimethylaminobenzaldehyde thiosemicarbazone: a simple novel selective and sensitive fluorescent sensor for mercury (II) in aqueous solution. *Talanta* **2006**, *69*, 103-106.
(27) Mahajan, P. G.; Dige, N. C.; Vanjare, B. D.; Phull, A. R.; Kim, S. J.; Lee, K. H. Gallotannin mediated silver colloidal nanoparticles as multifunctional nano platform: Rapid colorimetric and turn-on fluorescent sensor for Hg2+, catalytic and in vitro anticancer activities. *J. Lumin.* **2019**, *206*, 624-633.
(28) Hsieh, Y.-C.; Chir, J.-L.; Wu, H.-H.; Chang, P.-S.; Wu, A.-T. A sugar-aza-crown ether-based fluorescent sensor for Hg2+ and Cu2+. *Carbohydr. Res.* **2009**, *344*, 2236-2239.
(29) Vanjare, B. D.; Mahajan, P. G.; Ryoo, H.-I.; Dige, N. C.; Choi, N. G.; Han, Y.; Kim, S. J.; Kim, C.-H.; Lee, K. H. Novel rhodamine based chemosensor for detection of Hg2+: Nanomolar detection, real water sample analysis, and intracellular cell imaging. *Sens. Actuators B Chem.* **2021**, *330*, 129308.
(30) Bhalla, V.; Tejpal, R.; Kumar, M. Rhodamine appended terphenyl: A reversible "off–on" fluorescent chemosensor for mercury ions. *Sensors Actuators, B Chem.* **2010**, *151* (1), 180-185.
(31) Yuan, B.; Wang, D.-X.; Zhu, L.-N.; Lan, Y.-L.; Cheng, M.; Zhang, L.-M.; Chu, J.-Q.; Li, X.-Z.; Kong, D.-M. Dinuclear Hg II tetracarbene complex-triggered aggregation-induced emission for rapid and selective sensing of Hg 2+ and organomercury species. *Chem. Sci.* **2019**, *10*, 4220-4226.
(32) Lin, S.-Y.; Zhu, H.-J.; Xu, W.-J.; Wang, G.-M.; Fu, N.-Y. A squaraine based fluorescent probe for mercury ion via coordination induced deaggregation signaling. *Chin. Chem. Lett.* **2014**, *25*, 1291-1295.
(33) Wei, T.-b.; Gao, G.-y.; Qu, W.-j.; Shi, B.-b.; Lin, Q.; Yao, H.; Zhang, Y.-m. Selective fluorescent sensor for mercury (II) ion based on an easy to prepare double naphthalene Schiff base. *Sensors Actuators*, *B Chem.* **2014**, *199*, 142-147.
(34) Chen, S.; Wang, W.; Yan, M.; Tu, Q.; Chen, S.-W.; Li, T.; Yuan, M.-S.; Wang, J. 2-Hydroxy benzothiazole modified rhodol: aggregation-induced emission and dual-channel fluorescence sensing of Hg2+ and Ag+ ions. *Sensors Actuators*, *B Chem.* **2018**, *255*, 2086-2094.
(35) Zhang, R.; Chen, W. Nitrogen-doped carbon quantum dots: Facile synthesis and application as a "turn-off" fluorescent probe for detection of Hg2+ ions. *Biosens. Bioelectron.* **2014**, *55*, 83-90.
(36) Halder, S.; Mondal, J.; Ortega-Castro, J.; Frontera, A.; Roy, P. A Ni-based MOF for selective detection and removal of Hg 2+ in aqueous medium: a facile strategy. *Dalton Trans.* **2017**, *46*, 1943-1950.
(37) Moradi, E.; Rahimi, R.; Safarifard, V. Porphyrinic zirconium-based MOF with exposed pyrrole Lewis base site as an efficient fluorescence sensing for Hg2+ ions, DMF small

molecule, and adsorption of Hg2+ ions from water solution. *J. Solid State Chem. Sci.* **2020**, *286*, 121277.
(38) Hu, P.-P.; Liu, N.; Wu, K.-Y.; Zhai, L.-Y.; Xie, B.-P.; Sun, B.; Duan, W.-J.; Zhang, W.-H.; Chen, J.-X. Successive and specific detection of Hg2+ and I–by a DNA@ MOF biosensor: experimental and simulation studies. *Inorg. Chem.* **2018**, *57*, 8382-8389.
(39) Samanta, P.; Desai, A. V.; Sharma, S.; Chandra, P.; Ghosh, S. K. Selective recognition of Hg2+ ion in water by a functionalized metal–organic framework (MOF) based chemodosimeter. *Inorg. Chem.* **2018**, *57*, 2360-2364.
(40) Xia, T.; Song, T.; Zhang, G.; Cui, Y.; Yang, Y.; Wang, Z.; Qian, G. A terbium metal–organic framework for highly selective and sensitive luminescence sensing of Hg2+ ions in aqueous solution. *Chem. Eur. J.* **2016**, *22* (51), 18429-18434.
(41) Xu, X.-Y.; Yan, B. Fabrication and application of a ratiometric and colorimetric fluorescent probe for Hg 2+ based on dual-emissive metal–organic framework hybrids with carbon dots and Eu 3+. *J. Mater. Chem. C* **2016**, *4*, 1543-1549.
(42) Huang, N.-H.; Li, R.-T.; Fan, C.; Wu, K.-Y.; Zhang, Z.; Chen, J.-X. Rapid sequential detection of Hg2+ and biothiols by a probe DNA—MOF hybrid sensory system. *J. Inorg. Biochem.* **2019**, *197*, 110690.
(43) Radwan, A.; El-Sewify, I. M.; Shahat, A.; Azzazy, H. M.; Khalil, M. M.; El-Shahat, M. F. Multiuse Al-MOF chemosensors for visual detection and removal of mercury ions in water and skin-whitening cosmetics. *ACS Sustainable Chem. Eng.* **2020**, *8* (40), 15097-15107.
(44) Huang, N.-H.; Liu, Y.; Li, R.-T.; Chen, J.; Hu, P.-P.; Young, D. J.; Chen, J.-X.; Zhang, W.-H. Sequential Ag+/biothiol and synchronous Ag+/Hg 2+ biosensing with zwitterionic Cu 2+-based metal–organic frameworks. *Analyst* **2020**, *145*, 2779-2788.
(45) Wu, P.; Liu, Y.; Liu, Y.; Wang, J.; Li, Y.; Liu, W.; Wang, J. Cadmium-based metal–organic framework as a highly selective and sensitive ratiometric luminescent sensor for mercury (II). *Inorg. Chem.* **2015**, *54*, 11046-11048.
(46) Ponram, M.; Balijapalli, U.; Sambath, B.; Iyer, S. K.; Venkatachalapathy, B.; Cingaram, R.; Sundaramurthy, K. N. Development of paper-based chemosensor for the detection of mercury ions using mono-and tetra-sulfur bearing phenanthridines. *New J. Chem.* **2018**, (11), 8530-8536.
(47) Zhao, Y.; Xu, X.; Qiu, L.; Kang, X.; Wen, L.; Zhang, B. Metal–organic frameworks constructed from a new thiophene-functionalized dicarboxylate: luminescence sensing and pesticide removal. *ACS Appl. Mater. Interfaces* **2017**, *9* (17), 15164-15175.
(48) Yang, Y.; Ren, G.; Yang, W.; Qin, X.; Gu, D.; Liang, Z.; Guo, D.-Y.; Qinhe, P. A new MOF-based fluorescent sensor for the detection of nitrofuran antibiotics. *Polyhedron* **2021**, *194*, 114923.